PRP4K is a haploinsufficient tumour suppressor negatively regulated during epithelial-to-mesenchymal transition

Livia E. Clarke[1], Carter Van Iderstine[1], Sabateeshan Mathavarajah[1], Amit Bera[2], Moamen Bydoun[1], Allyson Cook[1], Stephen M. Lewis[2,3,4,5] and Graham Dellaire[1,5,6*]

1. Department of Pathology, Dalhousie University, Halifax, Nova Scotia, Canada
2. Atlantic Cancer Research Institute, Moncton, New Brunswick, E1C 8X3, Canada
3. Department of Chemistry & Biochemistry, Université de Moncton, Moncton, New Brunswick Canada
4. Department of Microbiology and Immunology, Dalhousie University, Halifax, Nova Scotia, Canada
5. Beatrice Hunter Cancer Research Institute, Halifax, Nova Scotia, Canada
6. Biochemistry and Molecular Biology, Dalhousie University, Halifax, Nova Scotia, Canada

*Corresponding Author:

Graham Dellaire, Ph.D.
Departments of Pathology and Biochemistry & Molecular Biology
Dalhousie University, P.O. BOX 15000
Halifax, Nova Scotia, Canada, B3H 4R2
Tel: (902)494-4730
Fax: (902)494-2519
E-mail: dellaire@dal.ca

Key words: PRP4K; PRPF4B; eIF3e; epithelial-to-mesenchymal transition (EMT); partial EMT; haploinsufficient tumour suppression; YAP

ABSTRACT

Reduced expression of haploinsufficient tumour suppressor genes is sufficient to alter cellular phenotypes towards carcinogenesis without complete loss of gene expression. As an essential gene, complete expression loss of pre-mRNA processing factor 4 kinase (PRP4K, also known as PRPF4B) is lethal. However, we demonstrate here that reduction of PRP4K levels by small interfering RNA in the mammary epithelial cell lines HMLE and MCF10A can induce partial epithelial-to-mesenchymal transition (EMT) marked by the retention of epithelial markers such as Zo-1 and E-cadherin, and upregulation of mesenchymal markers such as fibronectin and Zeb1. This partial EMT phenotype in non-transformed PRP4K-depleted cells is associated with greater invasive potential in 3D transwell assays, but either reduces or has no effect on 2D migration examined by scratch assay. This is in contrast to depletion of PRP4K in transformed triple-negative MDA-MB-231 breast cancer cells, which results in enhanced migration in 2D and invasion in 3D. Induction of EMT, using EMT-inducing media containing WNT-5a and TGF-β1 or depletion of eukaryotic translation initiation factor 3e (eIF3e) by shRNA, results in marked reduction of PRP4K expression. EMT induced by eIF3e depletion does not affect the transcription of PRP4K mRNA or turn-over of PRP4K protein, but rather reduces its protein translation. Finally, reduced PRP4K levels after eIF3e depletion correlated with increased YAP activity and nuclear localization, the latter being reversed by overexpression of exogenous PRP4K. Together, these data indicate that PRP4K is a haploinsufficient tumour suppressor negatively regulated by EMT, and that when depleted can induce partial EMT and increased cell invasion.

INTRODUCTION

Epithelial-to-mesenchymal transition (EMT) is an important process during embryonic development where cell-cell contacts are broken concurrent with loss of apical-basal polarity, and cytoskeletal reorganization, which converts immotile epithelial cells into motile mesenchymal cells [1]. The process of EMT is regulated by transcription factors like Zeb1 that induce the expression of mesenchymal genes, and like Snail/SNAI1 that repress the expression of epithelial genes such as E-cadherin [2]. The dysregulation of EMT also plays an important role in cancer progression and metastasis; the latter being the leading cause of cancer-related death [1, 3]. However, more recently partial or hybrid EMT states, where epithelial gene expression is maintained, have been described [4, 5]. Partial EMT appears to have several advantages over complete EMT, including the ability to promote collective migration of cancer cells, resistance to cell death, and increased plasticity and metastatic potential, all of which contribute to increased tumorigenicity [4, 5]. This is exemplified by the recent discovery that the maintenance of epithelial-like E-cadherin expression in mouse breast cancer models promotes cell survival during metastasis [6].

The overexpression of oncogenes and loss of genes encoding tumour suppressors are both linked to the incidence of cancer [7]. Although the complete loss of a tumour suppressor gene is common in the development of cancer, incomplete loss, termed haploinsufficiency, can be sufficient for tumour development in some cases [8, 9]. Several examples of haploinsufficient tumour suppressors exist including the phosphatase PTEN [10], the ribosomal protein RPL5 [11], the transcriptional regulator CUX1 [12], the motor protein KIF1Bβ [13] and the acetyltransferase CREBBP[14]. In these instances, there is typically 50% or greater loss of protein expression but even subtle changes in gene expression may affect tumour suppression.

For example, just a 20% decrease in PTEN protein expression can promote the development of cancer [10].

In this study, we identify the pre-mRNA processing factor 4 kinase (PRP4K, also known as *PRPF4B*) as a haploinsufficient tumour suppressor negatively regulated by EMT. PRP4K is an essential kinase that is highly conserved across species [15, 16]. PRP4K was initially described as *prp4* in *Schizosaccharomyces pombe*, which is a gene required for cell growth and regulation of pre-mRNA splicing in fission yeast [17, 18]. Characterization of the PRP4K homolog in mammals determined that it associates with the U5 small nuclear ribonucleoprotein (snRNP), and is required for the formation of spliceosomal complex B during pre-mRNA splicing [16, 19]. Although an essential gene in mammalian cells [20], reduced PRP4K expression is associated with poor outcomes in ovarian cancer [21]. Furthermore, partial loss of PRP4K expression has been implicated in cellular processes that impact tumour suppression and chemotherapy sensitivity [15]; these include regulation of the spindle assembly checkpoint [22] which impacts the cellular response to microtubule poisons including taxanes [23], transcriptional regulation [16, 24, 25], epidermal growth factor receptor (EGFR) signalling and anoikis [21], as well as Hippo/YAP signalling and cell migration [26]. Therefore, PRP4K can be broadly classified as a haploinsufficient tumour suppressor. Here we extend these findings by determining that when PRP4K is depleted by 50-90% by RNA interference, a partial EMT phenotype is induced in the non-transformed mammary epithelial cell lines MCF10A and HMLE, marked by upregulation of mesenchymal markers (Zeb1, fibronectin and vimentin) and retention of epithelial markers (E-cadherin, Zo-1 and claudin-1). Depletion of PRP4K in normal mammary epithelial cell lines generally inhibited cell migration in 2D, but promoted cell migration of transformed triple-negative breast cancer cell line MDA-MB-231. In addition, we

demonstrate that the induction of EMT in mammary epithelial cell lines promotes a decrease in PRP4K protein levels by affecting its translation, which correlated with increased YAP activity and nuclear localization, the latter being reversed by overexpression of exogenous PRP4K. Together, these data indicate that PRP4K is a haploinsufficient tumour suppressor negatively regulated by EMT, and that when depleted can induce partial EMT to promote more aggressive cancer phenotypes such as increased cell invasion.

MATERIALS AND METHODS

Cell Culture

All cell lines used in this study were confirmed mycoplasma-free by an in-house testing regimen (MycoAlert, Lonza; LT07-703). MDA-MB-231 cells from the American Type Culture Collection (ATCC; Gaithersburg, MD, USA) were cultured in Dulbecco's modified Eagle medium (DMEM; Sigma-Aldrich; Oakville, ON, CA) supplemented with 10% fetal calf serum, 1% penicillin/streptomycin at 37°C with 5% CO_2. HMLE (gift of Dr. Shashi Gujar, Dalhousie University) and MCF10A (ATCC) cells were cultured in Dulbecco's Modified Eagle's Medium/Nutrient Mixture F-12 (Sigma-Aldrich), supplemented with reagents from Sigma-Aldrich including: 5% horse serum, 1% penicillin/streptomycin, 0.5 µg/mL hydrocortisone, 10 µg/mL insulin, 10 ng/mL epidermal growth factor at 37°C with 5% CO_2. In addition, cholera toxin (1 ng/mL) (Sigma-Aldrich) was added to the MCF10A media.

For Actinomycin D treatment, cells were treated with 10 µg/ml Actinomycin D (Sigma-Aldrich) for the indicated time periods and then harvested for RT-qPCR analysis. For cycloheximide treatment, cells were treated with 50 µg/ml of cycloheximide (Sigma-Aldrich) for the indicated time periods and then harvested for Western blot analysis.

Lentiviral Transduction

To generate the MDA-MB-231, HMLE and MCF10A TRIPZ shPRP4K cell lines TRIPZ (shPRP4K-1 = clone: V2THS_383962, shPRP4K-2 = clone: V3THS_383960, Non-silencing shCTRL = RHS4743) lentiviral shRNAs were purchased from ThermoFisher Scientific (Thermo; Mississauga, ON, CA). Lentivirus was produced by co-transfection of the TRIPZ shRNA with pMD2.G and psPAX2 (gifts from Didier Trono, Addgene plasmid #12259 and

#12260, respectively) lentiviral packaging vectors into human HEK-293T cells via calcium-phosphate transfection (Promega; Madison, WI, USA), according to manufacturer's directions. After 48h, media from the transfected cells was filtered using a 0.45µ filter, and the viral media added to the target cell line for 48h. Following the 48h, the cells were split and treated with virus for another 48h to increase the transfection efficiency. Cells were allowed to recover in fresh media for 24h followed by selection in fresh medium containing 2µg/ml puromycin for 4 to 5 days. To induce expression of the inducible PRP4K shRNA, 5µg/mL doxycycline (Sigma-Aldrich) was added to culture media for 96 h prior to experimentation with the drug being replaced every 24 h.

Retroviral Transduction and Cell transfections

Production of MCF10A control and shEIF3E cell lines has been previously described [27]. MCF10A shCtrl and shEIF3E cell lines were transfected in 100 mm tissue culture plates with 5 µg of DNA at a ratio of 1:50 of a T7-tagged PRP4K expression vector [16] or pBluescript SK- (Stratagene/Agilent Technologies, Santa Clara, CA, USA) using the Neon Transfection System (Thermo) according to the manufacturer's directions. A pulse voltage of 1400V, pulse width of 20 ms and pulse number of 2 was used. Cells were harvested for RT-qPCR, and fixed and permeabilized for immunofluorescence 36 h post-transfection.

Induction of EMT by media supplementation

StemXVivo EMT Inducing Media Supplement was purchased from R&D Systems (Oakville, ON, CA). Cells were plated in 10 cm plates (HMLE- 5 x 10^5 cells; MCF10A- 1.5 x 10^6 cells) with 6 ml of complete media. Sixty microliters of 100X StemXVivo EMT Inducing Media

Supplement was added to each plate. Three days following cell plating, media was removed and replaced with fresh media and supplement. Two days later, plates were harvested for Western blot and RT-qPCR analysis.

Scratch Assay

Cells were seeded such that plates would be 90-100% confluent after 5 days. Twenty-four hours after plating the cells, doxycycline (5µg/mL; Sigma-Aldrich) was added to induce PRP4K knockdown and doxycycline was replaced every 24 hours. Seventy-two hours following doxycycline induction, media was replaced with low serum media (0.5%) to inhibit cell proliferation, and 24 h later a scratch was made using a P200 pipette tip. Wounds made by the scratch were imaged every 4 h and overall imaging time before wound closure was dependent on the cell line, with data presented up to 48 h. Wound area was calculated using ImageJ software (NIH, Bethesda, MA, USA) and migration rate was determined as a percentage of wound area reduction (wound closure) over time.

Transwell Assays

Growth factor-containing medium was added to the lower chamber and cells (MDA-MB-231: 5 x 10^4 (Migration [M]), 1 x 10^5 (Invasion [I]), HMLE: 1 x 10^5 (M & I), MCF10A: 2 x 10^5 (M & I)) reconstituted in serum-free medium were added to the upper chamber, which for migration assays were BioCoat™-Control-Cell-Culture inserts and for invasion assays were BioCoat™-Matrigel® inserts (Corning, Bedford, MA, USA) of 24-well plates. After 24 hours, the non-migratory cells on the inside of the insert were removed. Inserts were then washed with PBS and fixed with methanol for 15 minutes. Following fixation, inserts were washed with PBS and

stained with 0.5% crystal violet (Sigma-Aldrich) for 30 minutes. Inserts were then washed until clear of excess stain. Images of the inserts were taken using an Olympus CKX41 (Richmond Hill, ON, CA) equipped with ZEN lite 2012 acquisition software (Zeiss Canada, North York, ON, CA). For each replicate (n = 6), the number of migrating/invading cells in the insert was determined for 3-4 fields of view (2X magnification) and averaged.

Western Blot Analysis

Cells were lysed in ice-cold lysis buffer (20mM Tris-HCl pH8, 300mM KCl, 10% Glycerol, 0.25% Nonidet P-40, 0.5mM EDTA, 0.5mM EGTA, 1x protease inhibitors) and lysates cleared by centrifugation (25min, 15 000xg, 4°C) before polyacrylamide gel electrophoresis and Western blotting as previous described [10]. Primary antibodies used for Western blot analysis include anti-beta-actin (Sigma-Aldrich, A2228) (1:10000), anti-beta-tubulin (Santa Cruz [Santa Cruz, CA, USA], sc-9104) (1:5000), anti-claudin-1 (Cell Signaling [Danvers, MA, USA], 13255) (1:1000), anti-E-cadherin (Cell Signaling, 3195) (1:10000), anti-eIF3e (Abcam [Toronto, ON, CA], ab32419) (1:1000), anti-Fibronectin (Abcam, ab32419) (1:1000), anti-N-cadherin (Santa Cruz, sc-59987) (1:1000), anti-PRP4K (Novus Biologicals [Oakville, ON, CA], NBP1-82999) (1:5000), anti-Slug (Cell Signaling, 9585) (1:1000), anti-Snail (Cell Signaling, 3879) (1:1000), anti-T7 (Millipore [Oakville, ON, CA], ab3790) (1:1000), anti-Trk-B (Santa Cruz, sc-377218) (1:1000), anti-Vimentin (Cell Signaling, 5741) (1:1000), anti-Yap1 (Sigma-Aldrich, WH0010413M1) (1:1000), anti-Zeb-1 (Cell Signaling, 3396) (1:1000), and anti-Zo-1 (Cell Signaling, 8193) (1:1000). Secondary antibodies used include HRP-conjugated sheep anti-mouse IgG (Sigma-Aldrich, A5906) and HRP-conjugated goat anti-rabbit IgG (Sigma-Aldrich, A6154).

Immunofluorescence

Cells were plated onto sterile coverslips in 6-well plates and left to adhere overnight. Coverslips were washed with PBS for 5 minutes and then fixed in 4% paraformaldehyde for 30 minutes and permeabilized using 0.5% TritonX-100 (Sigma-Aldrich) for 5 minutes. Cells were washed again 3 times in PBS for 5 minutes each. Cells were blocked using 5% BSA (Bioshop; Burlington, ON, CA) in PBS for 20 minutes and then incubated with primary antibody for 1 hour at room temperature. Cells were washed 3 times with PBS for 5 minutes each and then incubated with Alexa Fluor secondary antibodies (Thermo) diluted 1:200 in 5% BSA (Bioshop) in PBS. Coverslips were washed 3 times with PBS for 5 minutes each, with 4',6-diamidino-2-phenylindole (DAPI)(Sigma-Aldrich) added to the second wash at to a concentration of 300 nM to counterstain DNA. Coverslips were mounted on frosted glass microscope slides using Dako mounting medium (Dako North America, Inc; Carpinteria, CA, USA) and allowed to dry overnight in the dark at room temperature. Images of immuno-stained cells were acquired using a custom-built Zeiss Cell Observer spinning-disk laser confocal microscope (Intelligent Imaging Innovations, 3i; Boulder, CO, USA) equipped with a 63X 1.4 N.A objective (Zeiss) and a Prime95B scientific CMOS camera and Slidebook 6 software (3i). Primary antibodies for immunofluorescence include mouse anti-Yap1 (Sigma-Aldrich, WH0010413M1)(1:33) and rabbit anti-T7 (Millipore, ab3790)(1:100). Secondary anti-mouse Alexa Fluor 555 and anti-rabbit Alexa Fluor 647 antibodies (ThermoFisher) were used at a dilution of 1:200.

RT-qPCR

Cell samples were lysed and homogenized using Trizol reagent (Thermo) according to the manufacturer's directions and samples were frozen at -80°C for further analysis. RNA was isolated using the Ambion PureLink RNA Mini Kit (Thermo) according to the manufacturer's protocol and included an on-column DNase I digestion. RNA quantity and quality were measured using a Nanodrop 2000 spectrophotometer (Thermo). Absorbance measurements A260/A280 and A260/A230 with ratios ~ 2.0 were accepted as pure for RNA. One microgram of RNA was reverse-transcribed to cDNA using the BioRad 5X iScript RT supermix kit (BioRad Laboratories Canada; Mississauga, ON, CA) for RT-qPCR, after which samples were diluted 1:1 with nuclease-free water. Samples without reverse transcriptase were included to confirm no genomic DNA contamination. Quantitative PCR (qPCR) was performed on cDNA samples using the 2X SsoAdvanced Universal SYBR Green Supermix (BioRad). A BioRad CFX Connect was used to perform the reactions and all experiments were done in triplicate. All primers used were designed using NCBI Primer Blast (https://www.ncbi.nlm.nih.gov/tools/primer-blast/). Gene expression data was normalized to at least two reference genes and analyzed using the BioRad CFX Maestro Software. Data were collected and analyzed as per the MIQE guidelines[28].

Puromycin incorporation Assay

To measure relative rates of PRP4K translation we employed a puromycin incorporation assay that relies on the detection of protein puromycylation[29, 30]. For this method, shCtrl and shEIF3E MCF10A cells were first grown in the absence of puromycin for 48 h prior to beginning the labelling with 10 μg/ml of puromycin for 2 h at 37 °C and 5% CO2. The cells were then harvested for detection of total puromycylated proteins as well as for immunoprecipitation (IP)

using 20 µl (~2-3 µg) of sheep anti-PRP4K antibody H143 [16]. IP was performed with the modified RIPA buffer. Briefly, after cold PBS washing, the MCF10A cells were lysed with IP lysis buffer (20 mM Tris, 350mM NaCl, 1mM EGTA, 1% NP-40) containing protease inhibitors for 30 min on ice. Next, lysed samples were centrifuged at 14 000 rpm for 20 min at 4 °C. After discarding the precipitate, the supernatants were collected and diluted the NaCl concentration to 150 mM to perform the IP. Cleared and diluted lysate was then incubated with the PRP4K antibody diluted in 0.5ml of PBS containing Dynabeads™ Protein G beads (Thermo) for 1 h, and incubated O/N at 4 °C. The next day precipitated complexes were washed with PBS two times, then washed with lysis buffer two times. The proteins were eluted with SDS sample buffer, boiled for 10 min and analyzed by SDS-PAGE as above, and nascent puromycylated proteins was detected by Western blot analysis as above using a mouse anti-puromycin antibody 12D10 (1:3000)(MABE343, Sigma-Aldrich).

YAP Nucleo-Cytoplasmic Intensity Ratio Determination

Images were taken at random fields of view and then quantified. Two methods of quantification were done; a ratio of nuclear-cytoplasm YAP signal and the observed relative distribution of YAP localization in terms of increased nuclear signal (N>C), more cytosolic (N<C) and similar signals between nuclear and cytosolic (N=C). A minimum of 50 cells were quantified for each replicate (3 replicates total) to determine the ratios and relative distributions of YAP. Signals were measured using ImageJ and then ratios were determined or used to determine the relative distribution of YAP within the cell.

Statistics

All graphs were made using GraphPad Prism 6. For conditions where two groups are being compared, a student's t-test was used (two-tailed). For experiments with three or more groups, a one-way ANOVA was carried out, employing Tukey's post-hoc analysis to determine significance between groups. Analysis of scratch assay was carried out using linear regression to determine differences in the slope of wound closure percentage over time (i.e. rate of wound healing) between groups. Finally, for the analysis of nuclear (N) vs cytoplasmic (C) ratios (i.e. N>C, N=C, N<C) the Freeman-Halton extension of the Fisher exact probability test for a two-row by three-column contingency table was used employing an online tool: http://vassarstats.net/fisher2x3.html.

RESULTS

Depletion of PRP4K in mammary epithelial cells induces partial EMT

Recently we demonstrated that depletion of PRP4K in transformed mouse ID8 ovarian and human MCF7 breast cancer cells leads to dysregulation of EGFR signalling and up-regulation of mesenchymal gene expression, including vimentin and fibronectin [21]. From these data we hypothesized that reduced PRP4K expression might lead to cancer progression by promoting EMT. To test this hypothesis, we chose to deplete PRP4K by doxycycline-inducible short hairpin RNA (shRNA) in the normal mammary epithelial cell lines HMLE and MCF10A, and the triple negative breast cancer (TNBC) cell line MDA-MB-231 (Fig 1). For each cell line, the level of PRP4K depletion ranged from 50 to 90%, with shPRP4K-2 having the greatest effect in each case. Upon induction of PRP4K shRNA we observed an increase in mesenchymal markers Zeb1 (2 to 9 fold) and fibronectin (2 to 5 fold) in all three cell lines, and cell-specific increases in Snail/SNAI1 (MDA-MB-231), Slug/SNAI2 (MDA-MB-231 and MCF10A), N-cadherin (HMLE) and vimentin (HMLE). Among the epithelial markers (E-cadherin, Claudin-1 and Zo-1), E-cadherin expression was most markedly decreased in the MDA-MB-231 TNBC cells (by 60-90%), was decreased strongly by only one hairpin in HMLE cells (by 80%), and only slightly decreased in the MCF10A cells (by 20%). Claudin-1 was decreased in the MDA-MB-231 cell line (by 60-80%), slightly decreased in the HMLE cells (by 30%) and strongly increased in the MCF10A cell line. For Zo-1 expression, protein levels were increased in the MDA-MB-231 cell line (by ~2-fold), and decreased in the HMLE and MCF10A cell lines (by 20-50%). Lastly, the mRNA expression of the same epithelial and mesenchymal factors did not consistently correlate with protein expression, suggesting post-transcriptional or post-translational control of these proteins following depletion of PRP4K (Supplemental Fig. S1).

Overall, mesenchymal marker expression was consistently increased with PRP4K depletion in all 3 cell lines, and in particular expression of fibronectin and Zeb1 were markedly increased in both transformed TNBC cells and non-transformed mammary epithelial cell lines. Epithelial marker expression was less consistent, but generally decreased in MDA-MB-231 cells, and either slightly reduced or increased in MCF10A and HMLE cells. These changes were off-set by reduced expression of mesenchymal genes like Snail/SNAI1 (in HMLE and MCF10A) and N-cadherin (MCF10A), and increases in epithelial markers such Zo-1 (in MDA-MB-231) and claudin-1 (in MCF10A); with the overall effect being a mix of both epithelial and mesenchymal gene expression consistent with a "partial" EMT phenotype [5], particularly in the non-transformed mammary epithelial cell lines.

Depletion of PRP4K promotes invasion of both tumorigenic and non-transformed mammary cell lines but has differential effects on cell migration

Given the role of EMT in aggressive cancer phenotypes, we sought to determine whether loss of PRP4K had an effect on the migratory and invasive potential of breast cancer cells and non-transformed mammary epithelial cell lines. To assess the migratory potential of cells, we first employed the 2D scratch assay (Fig. 2). Depletion of PRP4K increased the migratory potential of the MDA-MB-231 TNBC cell line in this assay, but had no effect on the HMLE cells and significantly decreased migration in the MCF10A cells (Fig. 2). These data indicate that the loss of PRP4K affects the migration of cells; however, the effect appears to be dependent on the transformation-state of the cell line, with more transformed and mesenchymal-like cells exhibiting increased 2D migration with loss of PRP4K.

We next conducted transwell assays with and without a matrigel-coated membrane to determine the invasive and migratory properties of the cells following PRP4K depletion, respectively. In the absence of matrigel, the migratory potential of the MDA-MB-231 cell line in this assay was increased for one shRNA (shPRP4K-2) but decreased in presence of the other (shPRP4K-1)(Fig. 3a). The migratory potential also decreased following PRP4K depletion in the HMLE cell line (Fig. 3b), but increased with PRP4K reduction in the MCF10A cell line (Fig 3c). In the presence of matrigel, the invasive potential of the MDA-MB-231 (Fig. 4a, shPRP4K-2) and MCF10A (Fig. 4c, both shPRP4K-1 and -2) cell lines increased following PRP4K knockdown. However, in the HMLE cell line, one shRNA with the greatest depletion of PRP4K (shPRP4K-2) significantly decreased the invasive potential of these cells (Fig 4b). Thus, depletion of PRP4K impacts 3D cell migration and invasion differently based on transformation-state and cell line. For example, depletion of PRP4K increases the migratory and invasive potential of MCF10A mammary epithelial cells in 3D culture, but decreases the migratory potential in 2D culture. This is in contrast to PRP4K-depleted MDA-MB-231 cells, which consistent with previous reports [26] showed increased migratory and invasive potential in both 2D and 3D culture.

The induction of EMT negatively regulates PRP4K protein expression

Given our data that depletion of PRP4K induces a partial EMT phenotype, which affects the 3D migratory and invasive potential of TNBC and non-transformed mammary epithelial cell lines, we next sought to determine whether the induction of EMT in non-transformed mammary epithelial cell lines affects the expression of PRP4K. Cells were cultured with an EMT-inducing media supplement consisting of various factors known to induce EMT (i.e. Wnt5a, TGFβ1, and

antibodies against E-cadherin, sFRP1, and Dkk1)[31] in both HMLE and MCF10A mammary epithelial cells. Following treatment with the supplement, both HMLE and MCF10A cells became more spindle-shaped (Fig 5a), consistent with a more mesenchymal phenotype, and exhibited increased mesenchymal gene expression (Fig 5c). Furthermore, the protein expression of PRP4K was decreased in both cell lines as compared to untreated cells, and this correlated with decreased E-cadherin and increased N-cadherin protein and gene expression, consistent with classical or "complete" EMT (Fig 5b and 5c). In addition, we observed significant increases in the expression of other mesenchymal genes, including *fibronectin* and *vimentin* in both cell lines (Fig 5c). Thus, these data indicate that induction of complete EMT, marked by loss of E-cadherin and upregulation of N-cadherin, can negatively regulate PRP4K protein expression.

We also sought to induce EMT through another method that did not rely on a cocktail of supplements, which in turn would allow more extensive characterization of mechanisms underlying the negative regulation of PRP4K during EMT. To this end, we chose to induce EMT by depletion of eukaryotic translation initiation factor 3e (eIF3e) in MCF10A cells. EIF3e is a non-essential subunit of the eIF3 translation initiation complex [32, 33], and previously we demonstrated that depletion of eIF3e induces a robust EMT phenotype in the MCF10A cell line [27]. When grown in culture, the MCF10A cells expressing a control shRNA (shCtrl) grew as tight clusters of well polarized epithelial cells (Fig 6a). Conversely, shRNA depletion of eIF3e using two different shRNAs induced a more mesenchymal phenotype characterized by single spindle-shaped cells, as previously described [27](Fig 6a). Transcript and protein analysis of various epithelial and mesenchymal markers again confirmed that eIF3e depletion robustly induced EMT (Fig 6b, 6d). This EMT phenotype also correlated with a 50-60% decrease in PRP4K protein expression (Fig 6b) but did not significantly alter PRP4K gene (*PRPF4B*)

expression (Fig 6c). Altogether, these data indicate that the induction of EMT negatively affects PRP4K protein expression and that regulation of PRP4K occurs by either a post-transcriptional mechanism or at the level of protein translation.

The induction of EMT by eIF3e depletion negatively regulates the translation of PRP4K

Since the induction of EMT by depletion of eIF3e negatively affected PRP4K protein expression but had no effect on PRP4K transcript expression, we next sought to determine if PRP4K was being regulated in a post-transcriptional or post-translational manner. First, we examined the transcript stability of the *PRPF4B* gene encoding PRP4K in control and eIF3e depleted MCF10A cells treated with actinomycin D to inhibit RNA synthesis followed by RT-qPCR to assess *PRPF4B* transcript decay over time, and found no differences in turn-over of the *PRPF4B* mRNA (Fig 7a). Next, we examined the protein stability and turn-over of the PRP4K protein after treatment of control and eIF3e-depleted MCF10A cells with cycloheximide to block new protein translation, assessing protein levels over various time points (Fig 7b). Rather seeing reduced levels of PRP4K overtime, the PRP4K protein appears to be stabilized after depletion of eIF3e compared to control MCF10A cells over the first 6 hours post-cycloheximide treatment (Fig 7b). These data indicate that during EMT induction by eIF3e depletion, PRP4K expression is not regulated at the level of mRNA or protein turn-over.

To assess how translation of PRP4K protein is altered during EMT induced by eIF3e depletion, we employed an assay based on the incorporation of puromycin into nascent proteins that has been used previously for assessment of translation by Western blot against puromycylated proteins [29, 30]. Using this assay, we found that we could readily detect puromycylated proteins in both control and eIF3e-depleted MCF10A cells (Fig 7c). Consistent

with previous studies [27], eIF3e-depleted cells exhibited reduced protein translation, as measured by reduced incorporation of puromycin in total protein compared to controls cells (Fig 7c). Upon immunoprecipitation, we could also detect robust puromycylation of PRP4K that was reduced by ~40% in the eIF3e-depleted cells compared to control when normalized to total immunoprecipitated PRP4K (Fig 7c). Thus these data indicate that, in the context of EMT induction by eIF3e depletion, changes in PRP4K protein expression are due to reduced translation.

Depletion of eIF3e in MCF10A cells correlates with nuclear accumulation of YAP and is reversed by overexpression of PRP4K

Following the observation that the induction of EMT negatively affects PRP4K protein expression, we next sought to investigate the cellular consequences of PRP4K loss. Cho and colleagues recently demonstrated that PRP4K can negatively regulate YAP nuclear accumulation; an event that correlated with inhibition of YAP-target genes, many of which are involved in the development of cancer [26]. Therefore, we hypothesized that negative regulation of PRP4K protein expression during EMT triggered by eIF3e depletion may similarly correlate with YAP nuclear accumulation and activation of YAP-mediated gene expression. To test this hypothesis, we examined the localization of YAP in control (shCtrl) and eIF3e depleted MCF10A cells, with and without overexpression of exogenous PRP4K tagged with a T7 epitope (Fig 8). We found that the nuclear to cytoplasmic ratio of YAP was higher in eIF3e-depleted cells (Fig 8) and this correlated with increased expression of YAP target genes, including *CTGF*, *ANKRD1*, and *CYR61* (Fig 9a). This nuclear accumulation of YAP was dependent on PRP4K expression, as add-back of T7-PRP4K resulted in a significant reduction in the nuclear to

cytoplasmic ratio of YAP (Fig 8). However, we did not see a significant effect on the expression of YAP target genes (i.e. *CTGF*, *ANKRD1* and *CYR61*) when T7-PRP4K was over-expressed both in control and eIF3e-depleted cells (Fig 9b). Thus, consistent with previous studies indicating that PRP4K regulates the nuclear accumulation of YAP [26], loss of PRP4K during EMT correlates with an increased nuclear to cytoplasmic YAP ratio, and overexpression of PRP4K reverses this phenotype in eIF3e-depleted MCF10A cells.

DISCUSSION

For more than three decades it has been recognized that epithelial-to-mesenchymal transition (EMT) plays a key role in the acquisition of aggressive cancer traits, such as the ability to metastasize, that drive malignancy. However, recent studies have linked aggressive cancer phenotypes to both mesenchymal-to-epithelial transition (MET) and developmental states caught "in-between" EMT and MET, otherwise known as partial EMT [1, 5, 34]. In this study, we examined the inter-relationship between EMT and PRP4K, a protein that when depleted can induce aggressive cancer phenotypes including anoikis and chemotherapy resistance [21, 23]. Our data indicate that the loss of PRP4K in "normal-like" mammary epithelial cell lines such as MCF10A and HMLE, promotes a partial EMT phenotype instead of a complete EMT process. This was demonstrated by the upregulation of key mesenchymal proteins such as fibronectin, vimentin and Zeb1, while retaining expression of epithelial protein markers including E-cadherin, Zo-1 and claudin-1 (Fig 1). Similarly, when PRP4K is depleted in the mesenchymal-like TNBC cell line MDA-MB-231, mesenchymal markers such as fibronectin, Zeb1, and Slug/SNAI2 were upregulated, as was epithelial marker Zo-1 by 2-fold (Fig 1). In previous work, we also observed the upregulation of Zeb1 following depletion of PRP4K in the epithelial-

like breast cancer cell line MCF7 but this occurred without loss of E-cadherin [21]. Thus, depletion of PRP4K seems to drive partial EMT in normal mammary epithelial cell lines (Fig 10A).

Since the acquisition of complete or partial EMT often provides cells with increased migratory and invasive potential [5], we hypothesized that loss of PRP4K might also increase the migratory and invasive potential of both normal and breast cancer cells. Using the scratch assay to assess the 2D migratory potential of cells, we found that loss of PRP4K significantly increased the 2D migration of MDA-MB-231 TNBC cells (Fig 2). However, these results were in stark contrast to the migratory behaviour of the HMLE and MCF10A cell lines after PRP4K loss, where depletion of PRP4K significantly inhibited 2D migration of MCF10A cells and had little effect on the migratory behaviour of HMLE cells (Fig 2). Thus, the effects of PRP4K depletion on cell migration under 2D culture conditions appears to be cell line and transformation-state dependent, with little effect on normal epithelial cells and transformed and mesenchymal-like cells exhibiting increased 2D migration. We next examined invasive and migratory potential of our cell lines in 3D culture conditions by employing transwell assays (Fig 3 and 4). In these studies, we found that depletion of PRP4K increased the migratory (Fig 3) and invasive potential (Fig 4) of both normal MCF10A mammary epithelial cells and TNBC cell line MDA-MBA-231 in 3D culture. However, both migration and invasion were inhibited in 3D culture conditions when PRP4K was depleted in HMLE cells. These data are not unique in showing a decoupling of migration in 2D and invasion properties in 3D culture conditions in relation to EMT, as previously it has been shown that induction of EMT in HMLE cells by overexpression of TWIST1 resulted in reduced 2D migration but increased invasion in the matrigel transwell assay [35].

Although our current study is the first to examine the impact of PRP4K depletion on the 2D and 3D migration and invasion behaviour of normal mammary epithelial cells, at least two other studies have looked at the effects of PRP4K depletion on cell migration using the MDA-MB-231 cell line. The first study, Cho *et al.*, determined that siRNA depletion of PRP4K increased migration in 2D employing the scratch assay over a 72 h time period, as well as increased invasion in 3D culture [26]. In contrast, Koedoot *et al.*, demonstrated reduced wound closure in the same 2D scratch assay over a 20 h time period when PRP4K was knocked down by siRNA in MDA-MB-231 cells [36]. Thus, our study is more aligned with the results of Cho and colleagues [26]. Differences between these studies include the width of the "wound" generated during the 2D scratch assay, as well as the length of evaluation time (72 h vs 20 h). One interpretation is that with a wider wound the effects of PRP4K depletion may take at least 48 h to be fully observed in regard to 2D migration, as we observed complete wound closure at 48 h (Fig 2). A second possibility is the off-target effects and/or efficiency of PRP4K depletion by shRNA or siRNA in these experiments. Indeed, we observed more profound effects on migration and invasion correlating with greater reduction in PRP4K protein levels (i.e. shPRP4K-2 shRNA, Fig 3 and 4). Overall, these findings indicate that loss of PRP4K can increase the migration and invasion of an already-transformed cell line in both 2D and 3D culture, but only increases the migration and invasion of normal epithelial cell lines like MCF10A in 3D culture conditions.

Since the induction of EMT can trigger gene expression changes that promote aggressive cancer phenotypes [1, 4], we next examined whether the induction of EMT affected the expression of PRP4K. Employing two different methods of EMT-induction involving either the exposure of cells to media containing WNT-5a and TGF-β1 (EMT-induction media[31], Fig 5),

as well as knockdown of eIF3e [27] (Fig 6), we determined that PRP4K protein expression is negatively regulated by the induction of complete EMT (as marked by dramatic loss of E-cadherin and upregulation of N-cadherin, Fig 5B and 6B) in MCF10A and HMLE cells; however, we found no effect on PRP4K transcript levels (Fig 5C and 6C). In particular, PRP4K protein expression was reduced between 50-60% by EMT induced by eIF3e depletion (Fig 6B). This was an intriguing result that led us to hypothesize that PRP4K is negatively regulated post-transcriptionally or post-translationally during the process of EMT. However, when we examined the transcript turn-over of the *PRPF4B* gene encoding PRP4K we did not observe any difference between control MCF10A cells or those in which EMT had been induced by depletion of eIF3e (Fig 7A). Similarly, we did not observe increased turn-over of the PRP4K protein after EMT induction in MCF10A cells (Fig 7B). This led us to evaluate PRP4K protein translation by immunoprecipitation and puromycin incorporation in control and eIF3e depleted MCF10A cells (Fig 7C). After induction of EMT by eIF3e depletion in MCF10A cells, we observed approximately 40% reduction in puromycylation of PRP4K, indicating that indeed PRP4K translation was reduced. Overall, these data indicate that PRP4K is negatively regulated at the level of translation following induction of complete EMT by depletion of eIF3e. One caveat in generalizing changes in PRP4K translation relative to EMT is that depletion of eIF3e alone may be responsible for reduced translation of PRP4K, rather than EMT *per se*. However, PRP4K transcript levels were not altered in either HMLE or MCF10A cells treated with EMT-induction media (Fig 5C), suggesting that post-transcriptional mechanisms such as translational control of PRP4K are likely a common feature of EMT in mammary cells.

Finally, the Hippo pathway is known to negatively regulate the transcription factors YAP and TAZ, which are upregulated in many cancer types and control transcriptional programs that

promote EMT and increased metastatic potential [37-39]. Cho and colleagues identified YAP as a substrate of PRP4K, which negatively regulates YAP by promoting its phosphorylation-dependent shuttling from the nucleus to the cytoplasm [26]. We observed that the induction of EMT by eIF3e depletion resulted in reduced expression of PRP4K (Fig 6B), which correlated with increased nuclear versus cytoplasmic localization of YAP (Fig 8) as well as increased expression of YAP target genes in MCF10A mammary epithelial cells (Fig 9A)(Summarized in Fig 10B). These data are reminiscent of the activation and nuclear accumulation of YAP/TAZ previously seen in the context of TGF-β1-mediated EMT in mouse mammary epithelial cell line NmuMG [40], which suggests that nuclear accumulation of YAP/TAZ is likely a general feature of EMT. We also observed that overexpression of PRP4K, to complement PRP4K loss in eIF3e-depleted cells, shifts the localization of YAP toward accumulation in the cytoplasm. However, overexpression of PRP4K in eIF3e-depleted cells did not significantly alter the expression of YAP target genes as compared to control MCF10A cells transfected with a non-expressing plasmid (i.e. pBluescript). One reason for this result could be that the stress of transfection alone could have a negative impact on YAP-mediated target gene expression as we observed much lower induction of YAP target genes (i.e. *CTGF*, *ANKRD1*, *CYR61*) in transfected (Fig 9B) versus non-transfected eIF3e-depleted MCF10A cells (Fig 9A). Nonetheless, our results are consistent with the findings of Cho *et al.*, [26] that PRP4K can regulate the nucleo-cytoplasmic shuttling of YAP, and as such, our data support a role for PRP4K loss in promoting the nuclear accumulation of YAP during EMT. In summary, this study provides further support for PRP4K as a haploinsufficient tumour suppressor, which we demonstrate here to be negatively regulated by EMT, and that when depleted can induce partial EMT to promote more aggressive cancer phenotypes including increased cell invasion.

ACKNOWLEDGMENTS

This work was funded by a Breast Cancer Society/QEII Foundation operating grant awarded to GD and an Operating Grant (#24135) from the Cancer Research Society and the Beatrice Hunter Cancer Research Institute (BHCRI) awarded to SML. GD and SML are Senior Scientist of the BHCRI, and both AC and LEC were supported by Cancer Research Training Program awards from the BHCRI with funds provided by CBCF – Atlantic, The Canadian Cancer Society, Nova Scotia Division as part of The Terry Fox Foundation Strategic Health Research Training (STIHR) Program in Cancer Research at the Canadian Institutes of Health Research (CIHR). SM is supported by a CGSM studentship from Natural Sciences and Engineering Research Council of Canada (NSERC), a Predoctoral Fellowship from the Killam Trusts, and a Scotia Scholar award from the Nova Scotia Health Research Foundation

Ethics declarations

Conflict of interest:

The authors declare that they have no conflict of interest.

REFERENCES

[1] Pradella D, Naro C, Sette C, Ghigna C. EMT and stemness: flexible processes tuned by alternative splicing in development and cancer progression. Mol Cancer. 2017;16:8.
[2] Skovierova H, Okajcekova T, Strnadel J, Vidomanova E, Halasova E. Molecular regulation of epithelial-to-mesenchymal transition in tumorigenesis (Review). Int J Mol Med. 2018;41:1187-200.
[3] Gupta GP, Massague J. Cancer metastasis: building a framework. Cell. 2006;127:679-95.
[4] Kim DH, Xing T, Yang Z, Dudek R, Lu Q, Chen YH. Epithelial Mesenchymal Transition in Embryonic Development, Tissue Repair and Cancer: A Comprehensive Overview. J Clin Med. 2017;7.
[5] Aiello NM, Maddipati R, Norgard RJ, Balli D, Li J, Yuan S, et al. EMT Subtype Influences Epithelial Plasticity and Mode of Cell Migration. Dev Cell. 2018;45:681-95 e4.
[6] Padmanaban V, Krol I, Suhail Y, Szczerba BM, Aceto N, Bader JS, et al. E-cadherin is required for metastasis in multiple models of breast cancer. Nature. 2019;573:439-44.
[7] Guo XE, Ngo B, Modrek AS, Lee WH. Targeting tumor suppressor networks for cancer therapeutics. Curr Drug Targets. 2014;15:2-16.
[8] Inoue K, Fry EA. Haploinsufficient tumor suppressor genes. Adv Med Biol. 2017;118:83-122.
[9] Santarosa M, Ashworth A. Haploinsufficiency for tumour suppressor genes: when you don't need to go all the way. Biochim Biophys Acta. 2004;1654:105-22.
[10] Alimonti A, Carracedo A, Clohessy JG, Trotman LC, Nardella C, Egia A, et al. Subtle variations in Pten dose determine cancer susceptibility. Nat Genet. 2010;42:454-8.
[11] Fancello L, Kampen KR, Hofman IJ, Verbeeck J, De Keersmaecker K. The ribosomal protein gene RPL5 is a haploinsufficient tumor suppressor in multiple cancer types. Oncotarget. 2017;8:14462-78.
[12] Arthur RK, An N, Khan S, McNerney ME. The haploinsufficient tumor suppressor, CUX1, acts as an analog transcriptional regulator that controls target genes through distal enhancers that loop to target promoters. Nucleic Acids Res. 2017;45:6350-61.
[13] Ando K, Yokochi T, Mukai A, Wei G, Li Y, Kramer S, et al. Tumor suppressor KIF1Bbeta regulates mitochondrial apoptosis in collaboration with YME1L1. Mol Carcinog. 2019;58:1134-44.
[14] Zhang J, Vlasevska S, Wells VA, Nataraj S, Holmes AB, Duval R, et al. The CREBBP Acetyltransferase Is a Haploinsufficient Tumor Suppressor in B-cell Lymphoma. Cancer Discov. 2017;7:322-37.
[15] Corkery DP, Holly AC, Lahsaee S, Dellaire G. Connecting the speckles: Splicing kinases and their role in tumorigenesis and treatment response. Nucleus. 2015;6:279-88.
[16] Dellaire G, Makarov EM, Cowger JJ, Longman D, Sutherland HG, Luhrmann R, et al. Mammalian PRP4 kinase copurifies and interacts with components of both the U5 snRNP and the N-CoR deacetylase complexes. Mol Cell Biol. 2002;22:5141-56.
[17] Alahari SK, Schmidt H, Kaufer NF. The fission yeast prp4+ gene involved in pre-mRNA splicing codes for a predicted serine/threonine kinase and is essential for growth. Nucleic Acids Res. 1993;21:4079-83.

[18] Rosenberg GH, Alahari SK, Kaufer NF. prp4 from Schizosaccharomyces pombe, a mutant deficient in pre-mRNA splicing isolated using genes containing artificial introns. Mol Gen Genet. 1991;226:305-9.
[19] Schneider M, Hsiao HH, Will CL, Giet R, Urlaub H, Luhrmann R. Human PRP4 kinase is required for stable tri-snRNP association during spliceosomal B complex formation. Nat Struct Mol Biol. 2010;17:216-21.
[20] Hart T, Chandrashekhar M, Aregger M, Steinhart Z, Brown KR, MacLeod G, et al. High-Resolution CRISPR Screens Reveal Fitness Genes and Genotype-Specific Cancer Liabilities. Cell. 2015;163:1515-26.
[21] Corkery DP, Clarke LE, Gebremeskel S, Salsman J, Pinder J, Le Page C, et al. Loss of PRP4K drives anoikis resistance in part by dysregulation of epidermal growth factor receptor endosomal trafficking. Oncogene. 2018;37:174-84.
[22] Montembault E, Dutertre S, Prigent C, Giet R. PRP4 is a spindle assembly checkpoint protein required for MPS1, MAD1, and MAD2 localization to the kinetochores. J Cell Biol. 2007;179:601-9.
[23] Corkery DP, Le Page C, Meunier L, Provencher D, Mes-Masson AM, Dellaire G. PRP4K is a HER2-regulated modifier of taxane sensitivity. Cell Cycle. 2015;14:1059-69.
[24] Huang Y, Deng T, Winston BW. Characterization of hPRP4 kinase activation: potential role in signaling. Biochem Biophys Res Commun. 2000;271:456-63.
[25] Huang B, Ahn YT, McPherson L, Clayberger C, Krensky AM. Interaction of PRP4 with Kruppel-like factor 13 regulates CCL5 transcription. J Immunol. 2007;178:7081-7.
[26] Cho YS, Zhu J, Li S, Wang B, Han Y, Jiang J. Regulation of Yki/Yap subcellular localization and Hpo signaling by a nuclear kinase PRP4K. Nat Commun. 2018;9:1657.
[27] Gillis LD, Lewis SM. Decreased eIF3e/Int6 expression causes epithelial-to-mesenchymal transition in breast epithelial cells. Oncogene. 2013;32:3598-605.
[28] Bustin SA, Benes V, Garson JA, Hellemans J, Huggett J, Kubista M, et al. The MIQE guidelines: minimum information for publication of quantitative real-time PCR experiments. Clin Chem. 2009;55:611-22.
[29] David A, Dolan BP, Hickman HD, Knowlton JJ, Clavarino G, Pierre P, et al. Nuclear translation visualized by ribosome-bound nascent chain puromycylation. J Cell Biol. 2012;197:45-57.
[30] Schmidt EK, Clavarino G, Ceppi M, Pierre P. SUnSET, a nonradioactive method to monitor protein synthesis. Nat Methods. 2009;6:275-7.
[31] Scheel C, Eaton EN, Li SH, Chaffer CL, Reinhardt F, Kah KJ, et al. Paracrine and autocrine signals induce and maintain mesenchymal and stem cell states in the breast. Cell. 2011;145:926-40.
[32] Zhou C, Arslan F, Wee S, Krishnan S, Ivanov AR, Oliva A, et al. PCI proteins eIF3e and eIF3m define distinct translation initiation factor 3 complexes. BMC Biol. 2005;3:14.
[33] Masutani M, Sonenberg N, Yokoyama S, Imataka H. Reconstitution reveals the functional core of mammalian eIF3. EMBO J. 2007;26:3373-83.
[34] Diepenbruck M, Christofori G. Epithelial-mesenchymal transition (EMT) and metastasis: yes, no, maybe? Curr Opin Cell Biol. 2016;43:7-13.
[35] Schaeffer D, Somarelli JA, Hanna G, Palmer GM, Garcia-Blanco MA. Cellular migration and invasion uncoupled: increased migration is not an inexorable consequence of epithelial-to-mesenchymal transition. Mol Cell Biol. 2014;34:3486-99.

[36] Koedoot E, Fokkelman M, Rogkoti VM, Smid M, van de Sandt I, de Bont H, et al. Uncovering the signaling landscape controlling breast cancer cell migration identifies novel metastasis driver genes. Nat Commun. 2019;10:2983.
[37] Lei QY, Zhang H, Zhao B, Zha ZY, Bai F, Pei XH, et al. TAZ promotes cell proliferation and epithelial-mesenchymal transition and is inhibited by the hippo pathway. Mol Cell Biol. 2008;28:2426-36.
[38] Shao DD, Xue W, Krall EB, Bhutkar A, Piccioni F, Wang X, et al. KRAS and YAP1 converge to regulate EMT and tumor survival. Cell. 2014;158:171-84.
[39] Noguchi S, Saito A, Nagase T. YAP/TAZ Signaling as a Molecular Link between Fibrosis and Cancer. Int J Mol Sci. 2018;19.
[40] Diepenbruck M, Waldmeier L, Ivanek R, Berninger P, Arnold P, van Nimwegen E, et al. Tead2 expression levels control the subcellular distribution of Yap and Taz, zyxin expression and epithelial-mesenchymal transition. J Cell Sci. 2014;127:1523-36.

FIGURE LEGENDS

Figure 1: Loss of PRP4K induces a partial EMT at the protein level. Whole-cell lysates of MDA-MB-231, HMLE, and MCF10A control (shCtrl) and PRP4K depleted (shPRP4K-1 and shPRP4K-2) cells were prepared and subject to Western blot analysis of epithelial (E-cadherin, Zo-1, claudin-1) and mesenchymal (Snail, Slug, Zeb1, Trk-B, N-cadherin, Vimentin, Fibronectin) proteins as indicated. Ratios of protein level, normalized to actin, are shown below each row of Western blots relative to either shCtrl levels (set to 1) or lowest expression in PRP4K-depleted cells.

Figure 2: Effects of PRP4K depletion on the migration of normal mammary and transformed TNBC cells measured by wound healing scratch assay. (**A**) Normal mammary epithelial (MCF10A, HMLE) or TNBC MDA-MB-231 control (shCtrl) and PRP4K-depleted (shPRP4K-1 and shPRP4K-2) cells were grown to confluency and then a scratch was made using a P200 pipette tip and the average area of the scratch was set to a value of one and imaged every 4 h, and relative area of the scratched area plotted over 48 h. N = 3, error bars= SEM. Significance was determined by a linear regression comparing slopes between shCtrl and both shPRP4K hairpins. (**B**) Representative images of the scratched area measured in (A) shown over time.

Figure 3: Effects of PRP4K depletion on the migration of normal mammary and transformed TNBC cells measured by transwell assay. (**A-C**) TNBC MDA-MB-231 or normal mammary epithelial (HMLE, MCF10A) control (shCtrl) and PRP4K-depleted (shPRP4K-1 and shPRP4K-2) cells were plated in transwells and migration into the insert

membrane was determined 24 h later by visual enumeration and depicted as a bar graph (left), with representative images of each insert shown (right). Arrow heads indicate position HMLE and MCF10A cells that have migrated into the insert membrane. N = 6, error bars = SEM. Significance was determined by a one-way ANOVA. *p<0.05, **p<0.01, ***p<0.001, ****p<0.0001

Figure 4. Effects of PRP4K depletion on the 3D invasion of normal mammary and transformed TNBC cells measured by matrigel transwell assay. (**A-C**) TNBC MDA-MB-231 or normal mammary epithelial (HMLE, MCF10A) control (shCtrl) and PRP4K depleted (shPRP4K-1 and shPRP4K-2) cells were plated in matrigel coated transwells and 3D invasion through the matrigel into the insert membrane was determined 24 h later by visual enumeration and depicted as a bar graph (left), with representative images of each insert shown (right). Arrow heads indicate position of HMLE and MCF10A cells that invaded the insert membrane. N = 6 experiments, error bars = SEM. Significance was determined by a one-way ANOVA. **p<0.01, ****p<0.0001.

Figure 5. The induction of EMT decreases PRP4K protein expression in HMLE and MCF10A cells. A) Phase contrast micrographs of MCF10A and HMLE cells treated with (+EMT) or without (WT) EMT-induction media for 5 days. **B**) Western blot analysis of PRP4K protein expression from whole cell lysates prepared from cells treated with EMT-induction media as in A. **C**) Quantitative PCR of cDNA prepared from cells treated with EMT-induction media as in A, with data normalized to at least two reference genes as indicated. N = 3, error bars= SEM. Significance was determined by a t-test. *=p<0.05.

Figure 6. The induction of EMT by depletion of eIF3e decreases PRP4K protein expression in MCF10A cells. A) Phase contrast micrographs of control (shCtrl) and eIF3e-depleted cells (shEIF3E-1 and shEIF3-2). **B**) Western blot analysis of whole cell lysates of MCF10A shCtrl and shEIF3E cells for markers of EMT as indicated. **C**) Quantitative PCR of PRP4K gene (*PRPF4B*) mRNA expression in MCF10A shCtrl and shEIF3E cells. **D**) Quantitative PCR analysis of EMT-associated gene expression (as indicated) in MCF10A shCtrl and shEIF3E cells. N = 3, error bars= SEM. Significance was determined by a t-test. *=$p<0.05$, **=$p<0.01$, ***=$p<0.001$.

Figure 7. The induction of EMT by depletion of eIF3e negatively regulates the translation of PRP4K in MCF10A cells. A) Quantitative PCR of PRP4K gene (*PRPF4B*) mRNA expression in control (shCtrl) and eIF3e-depleted (shEIF3E-1 and shEIF3-2) MCF10A cells treated with 10 µg/mL Actinomycin D for the indicated time periods, with data normalized to at least two reference genes as indicated. N = 3, error bars= SEM. Significance was determined by a one-way ANOVA. **B**) Western blot analysis of whole cell lysates of MCF10A shCtrl and shEIF3E cells treated with 50µg/mL cycloheximide for the indicated time periods. **C**) Puromycin incorporation assay of MCF10A shCtrl and shEIF3E cells. Cells were grown for 24 h without puromycin selection and then pulsed with puromycin prior to Western blot analysis of total cell lysates (left) or following immunoprecipitation (IP) of PRP4K and detection of puromycylation of proteins and PRP4K (right).

Figure 8. Depletion of eIF3e in MCF10A cells increases YAP nuclear localization and is reversed by overexpression of PRP4K. A) Immunofluorescence images of control (shCtrl) and eIF3e-depleted MCF10A cells (shEIF3E-1 and shEIF3-2) transfected with pBluescript SK- (mock) or T7-tagged PRP4K (T7-PRP4K) plasmids. An enlarged region of each merged micrograph, bound by the white box, is shown in the far right panel. DAPI=blue, YAP=green, T7=red. Scale bars = 10 microns. **B**) Histogram of YAP nuclear-cytoplasmic ratios for shCtrl and shEIF3E cells transfected with pBluescript SK- (-) or with (+) T7-tagged PRP4K. N = 3, error bars=SEM. Significance was determined by a one-way ANOVA. **C**) Graph showing the percentage of cells in B with N<C, N=C and N>C expression of YAP. Significance was determined by a Fisher's exact test. **=p<0.01, ***=p<0.001, ****=p<0.0001.

Figure 9. Overexpression of PRP4K does not increase the expression of YAP target genes in eIF3e-depleted MCF10A cells. A) Quantitative PCR analysis of cDNA prepared from control (shCtrl) and eIF3e-depleted cells (shEIF3E-1 and shEIF3-2), with data normalized to at least two reference genes as indicated. N = 3, error bars= SEM. Significance was determined by a one-way ANOVA. **B**) Quantitative PCR analysis of cDNA prepared from control (shCtrl) and eIF3e-depleted cells (shEIF3E-1 and shEIF3-2) transfected with pBluescript SK- (pBSK) or T7-tagged PRP4K, with data normalized to at least two reference genes as indicated. N = 3, error bars= SEM. Significance was determined by a one-way ANOVA. *=p<0.05, **=p<0.01.

Figure 10. Overview of the key findings on the relationship between PRP4K and EMT.

A) Epithelial-to-mesenchymal transition (EMT) occurs over a spectrum of phenotypes and loss of PRP4K in the mammary epithelial cells promotes a partial EMT phenotype that increases cell invasion potential. **B**) Model of the effects of eIF3e depletion on PRP4K levels and YAP localization in MCF10A cells. i) Depletion of eIF3e induces EMT. ii) EMT induction through eIF3e depletion reduces PRP4K protein translation, which is correlated with increased YAP activity and nuclear localization. iii) Overexpression of PRP4K inhibits the nuclear localization of YAP. Elements of this figure were created with BioRender.com.

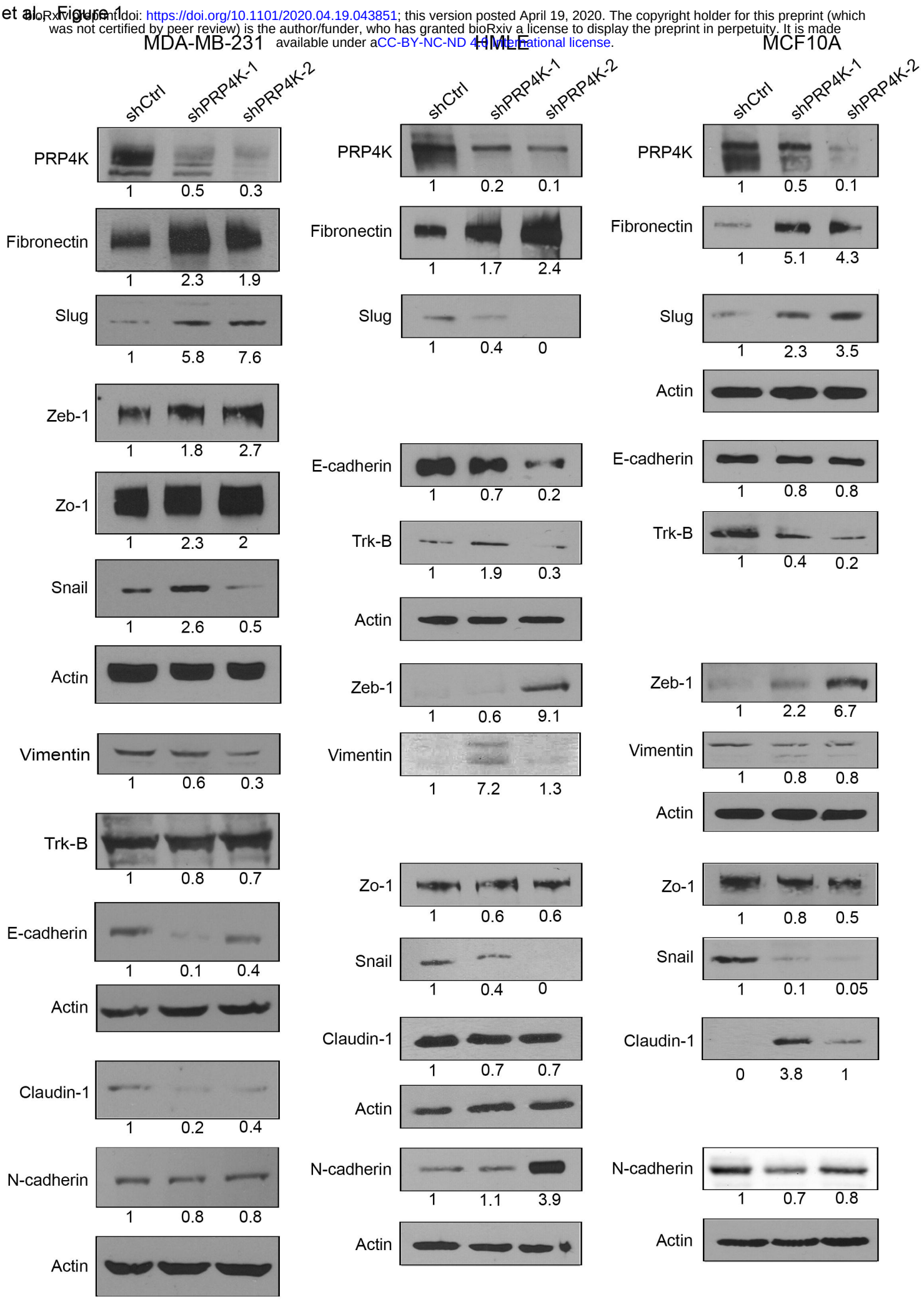

A

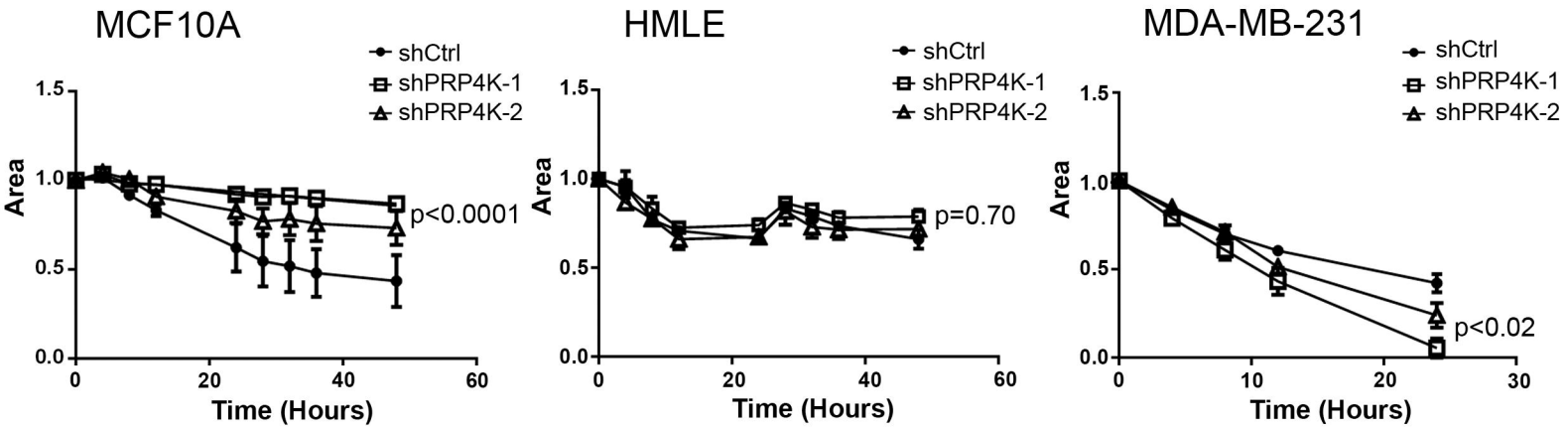

B

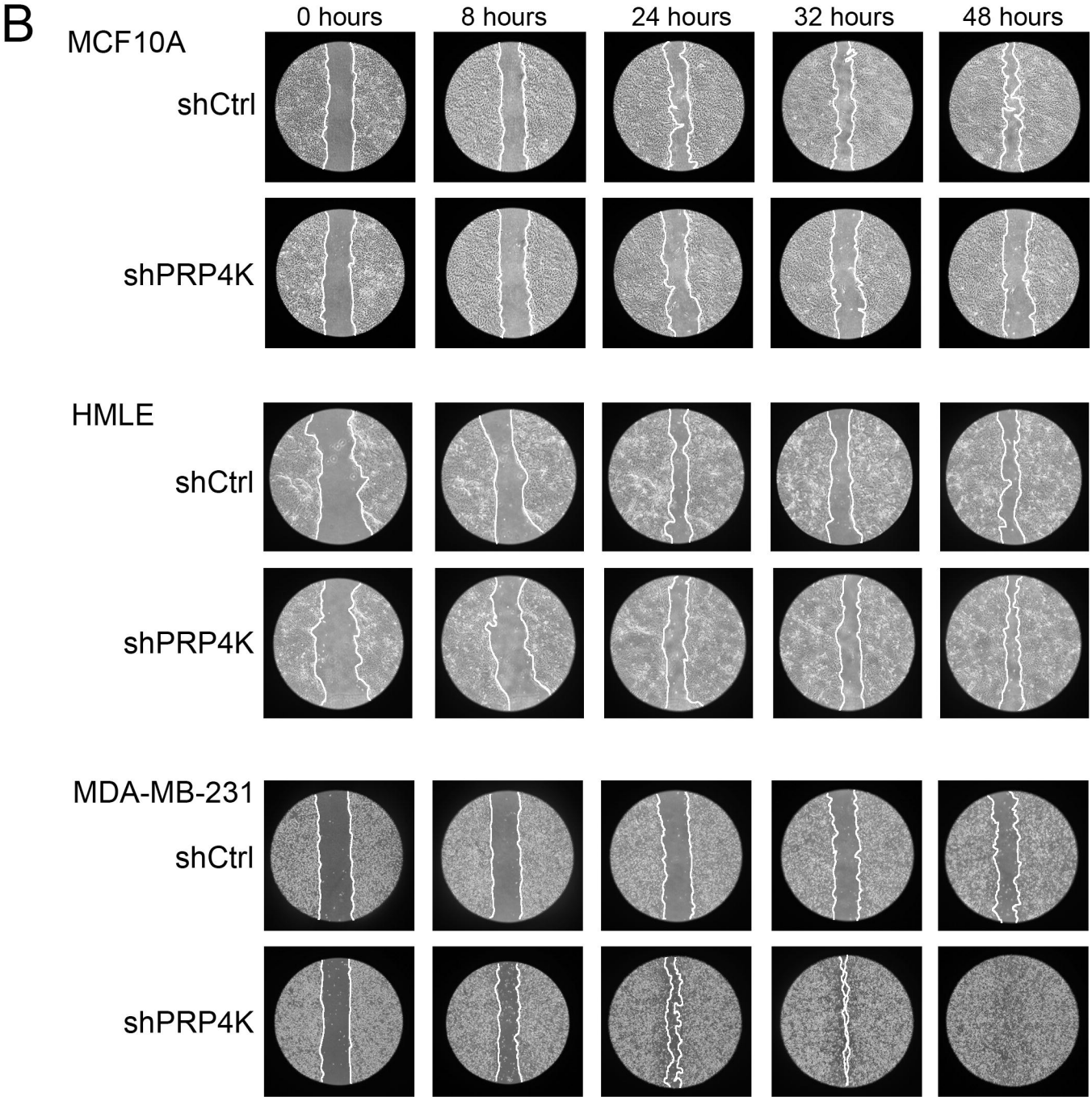

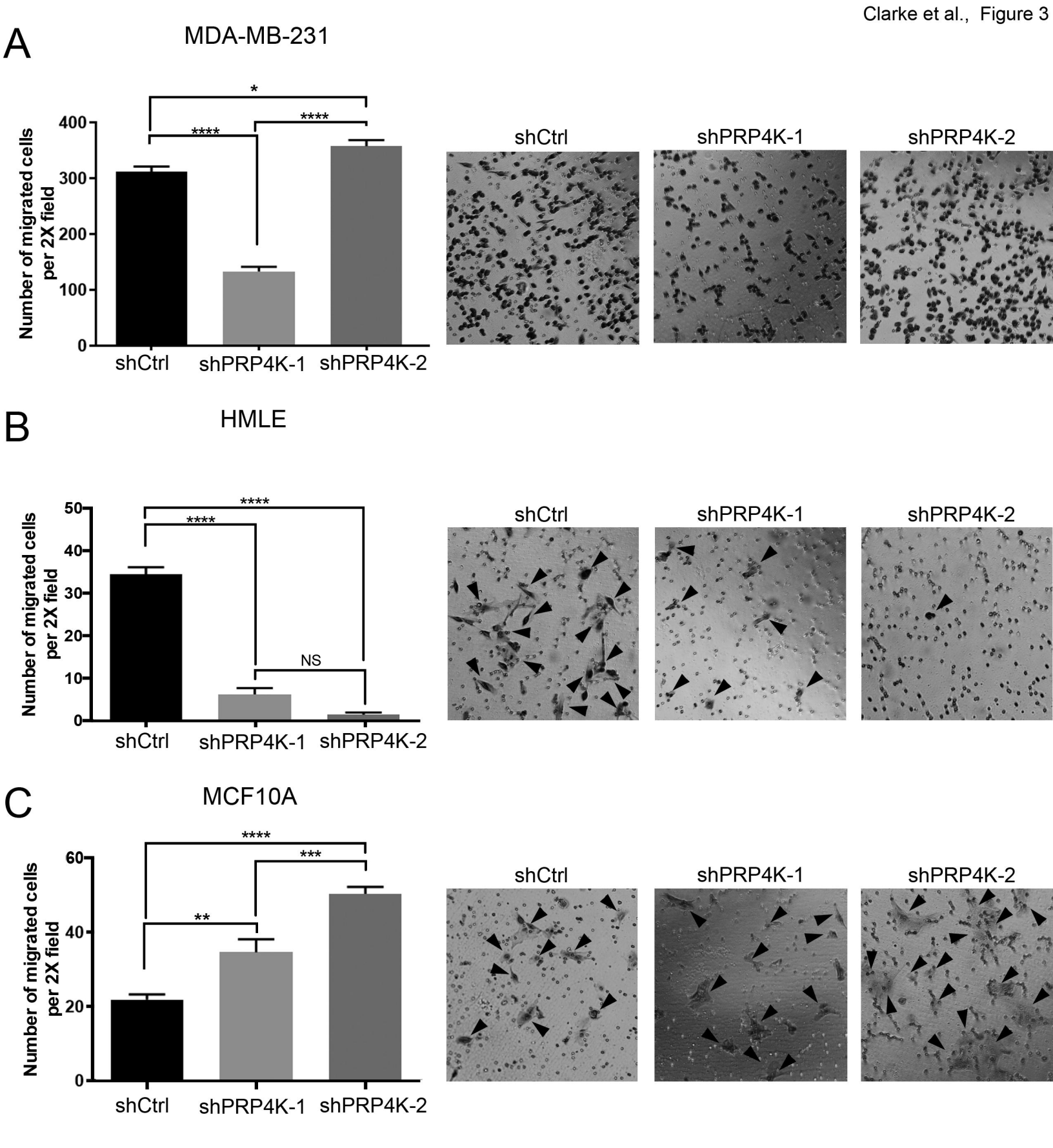
A
MDA-MB-231
Number of migrated cells per 2X field
400
300
200
100
0
*
****
****
shCtrl
shPRP4K-1
shPRP4K-2
shCtrl
shPRP4K-1
shPRP4K-2
B
HMLE
Number of migrated cells per 2X field
50
40
30
20
10
0
****
****
NS
shCtrl
shPRP4K-1
shPRP4K-2
shCtrl
shPRP4K-1
shPRP4K-2
C
MCF10A
Number of migrated cells per 2X field
60
40
20
0
****
***
**
shCtrl
shPRP4K-1
shPRP4K-2
shCtrl
shPRP4K-1
shPRP4K-2

A

MDA-MB-231

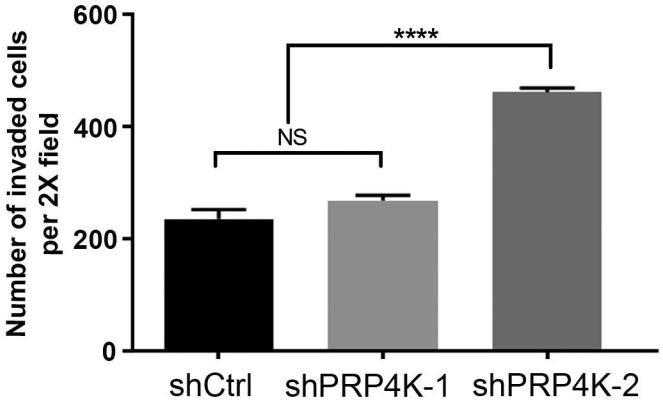

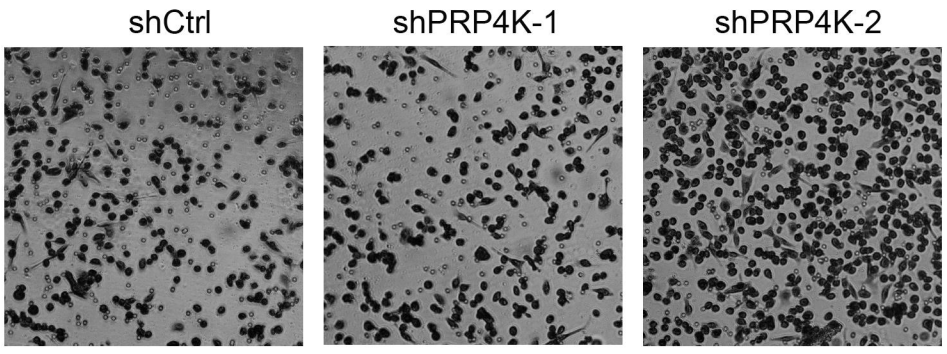

B

HMLE

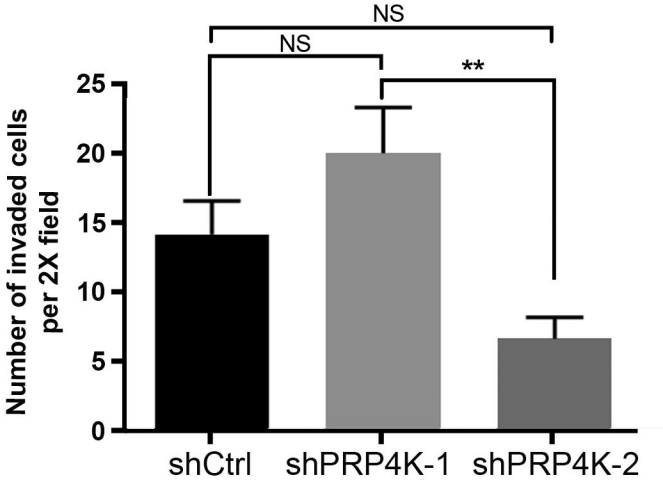

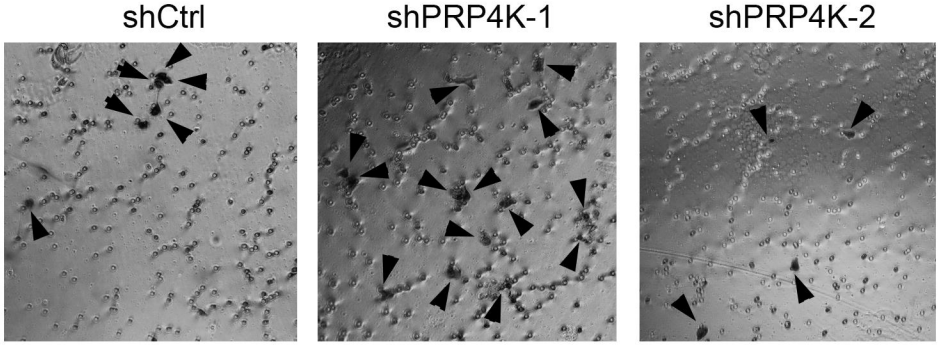

C

MCF10A

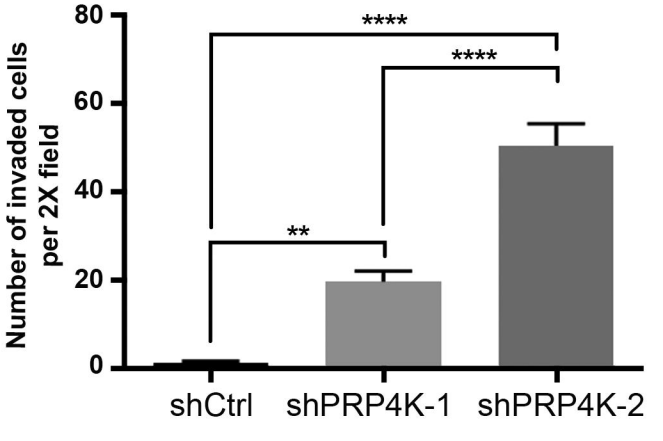

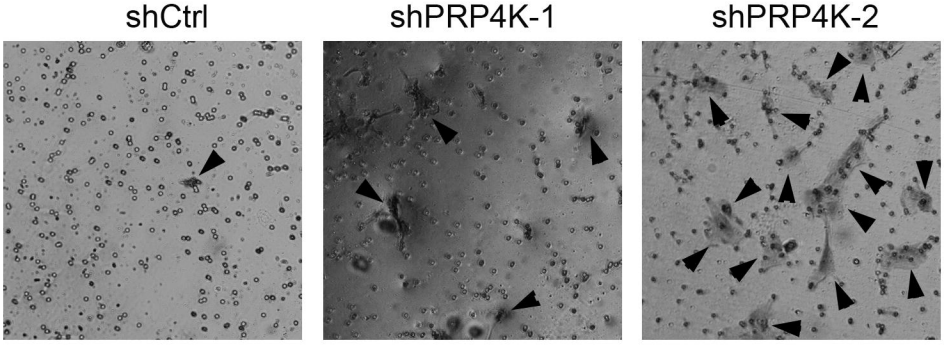

A

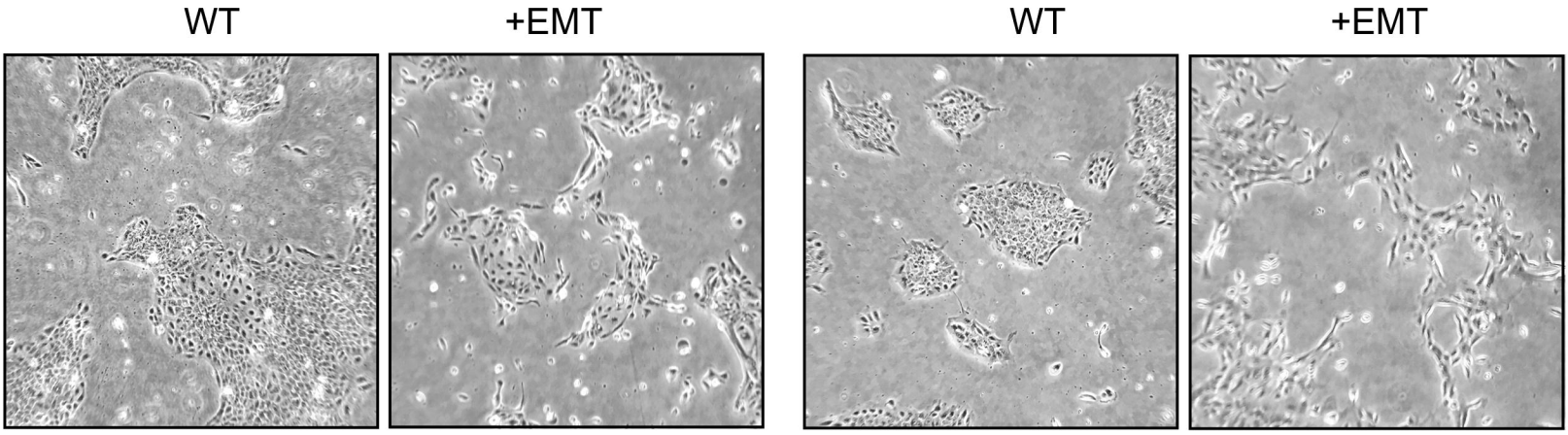

B

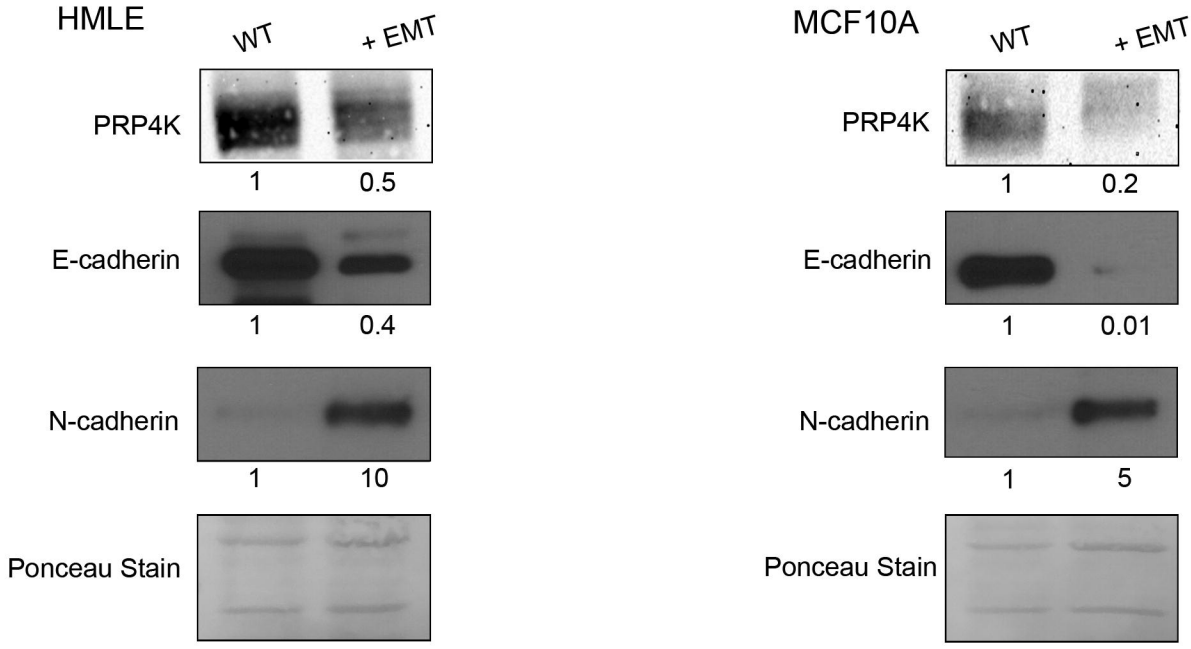

C

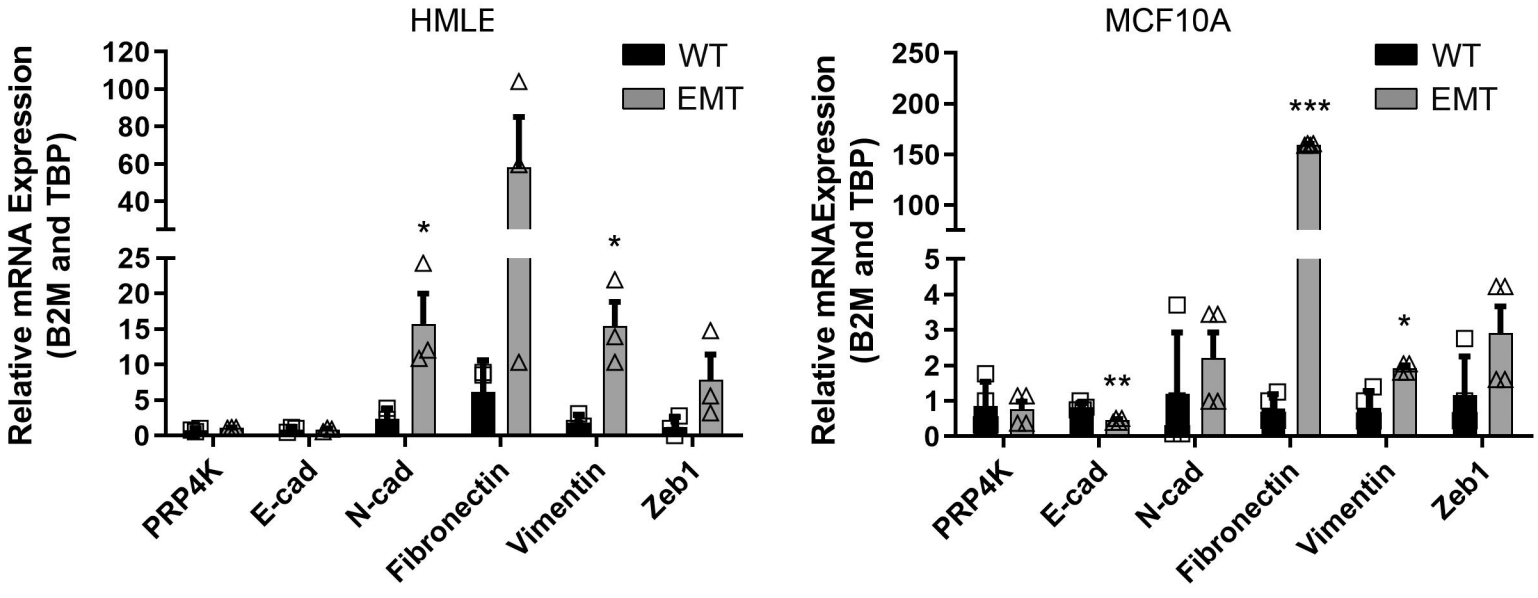

A

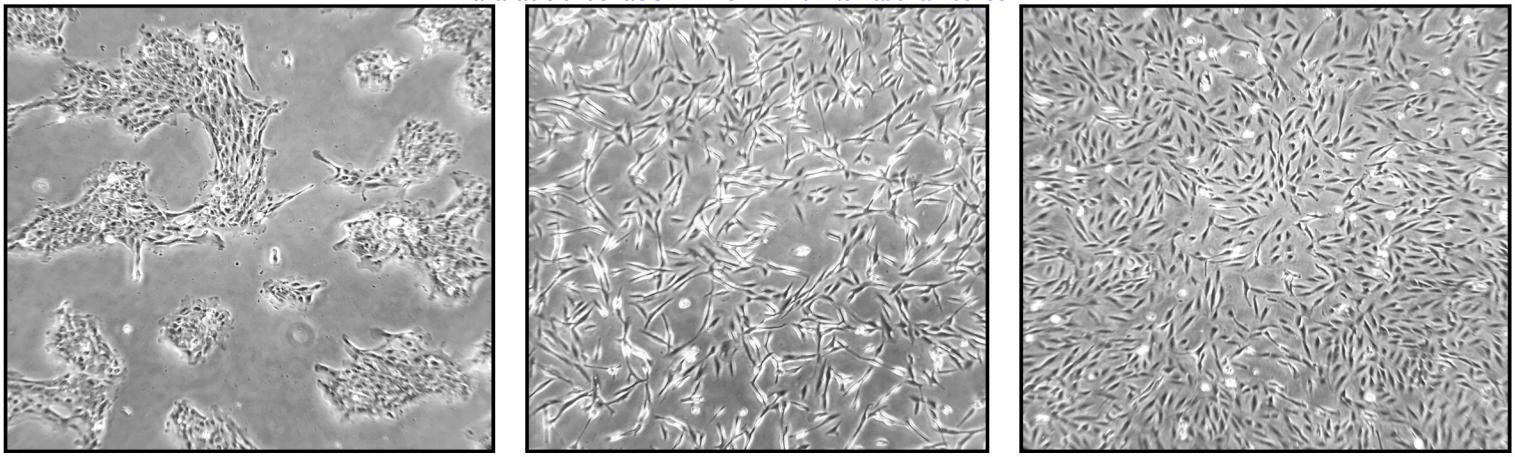

B

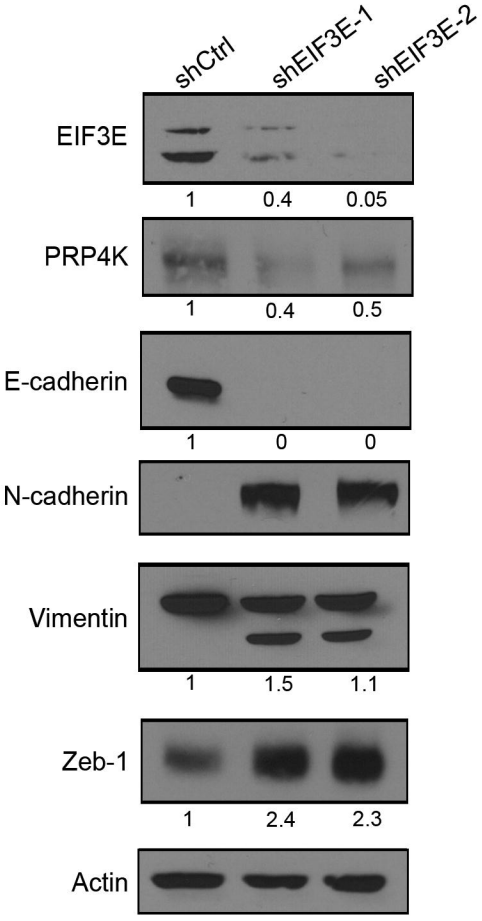

C

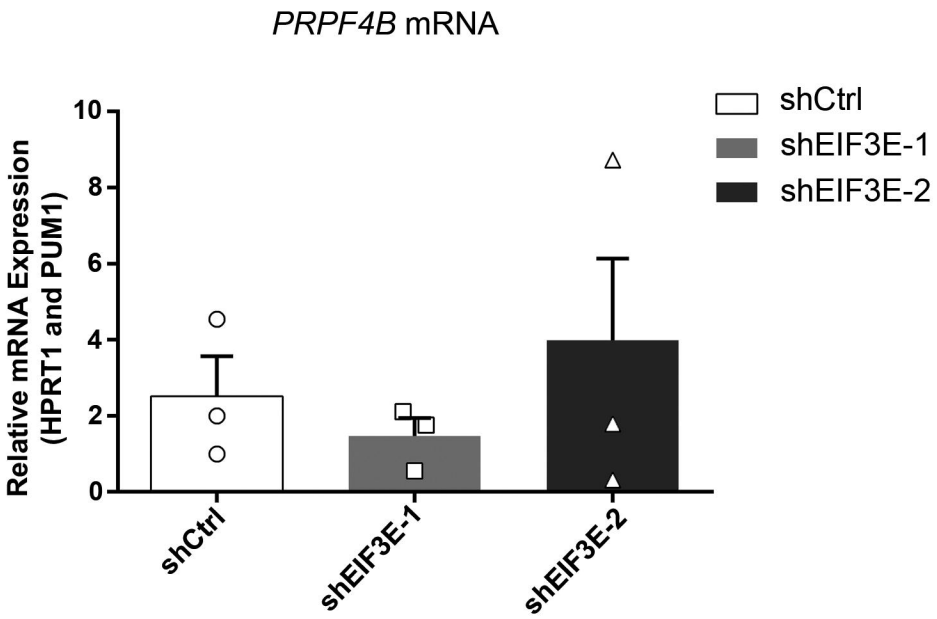

D

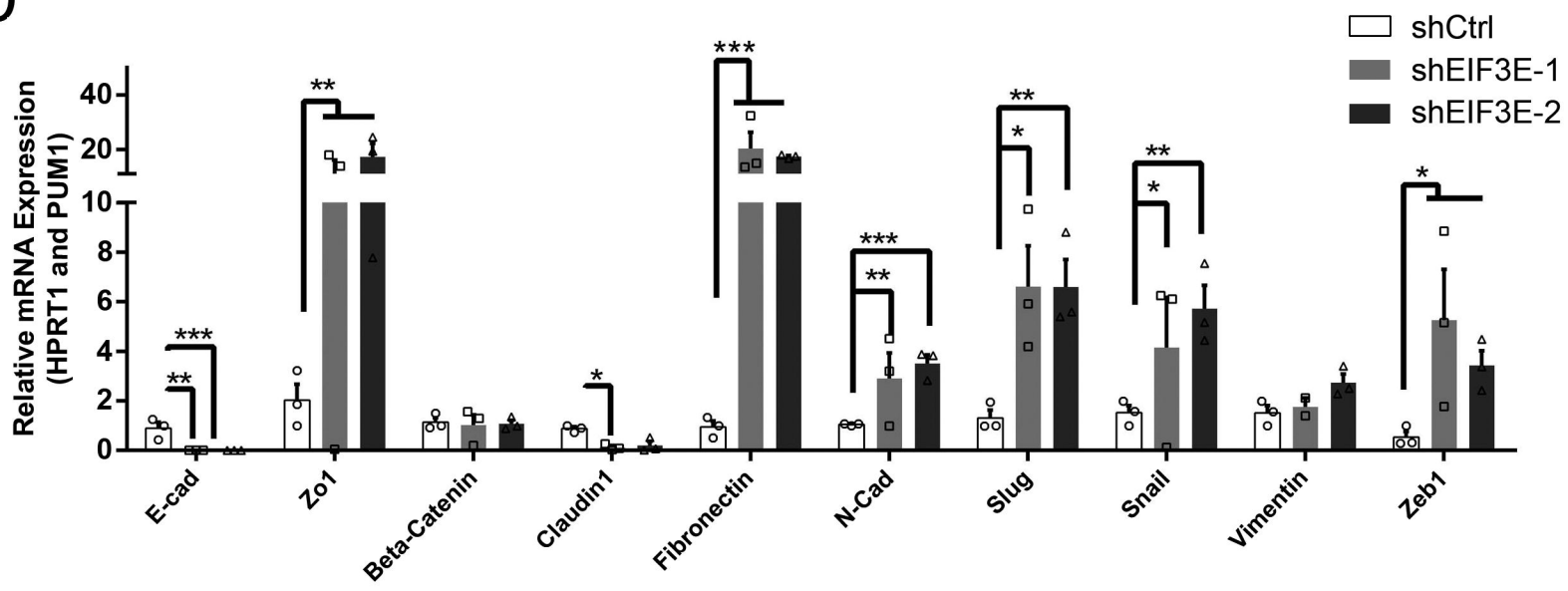

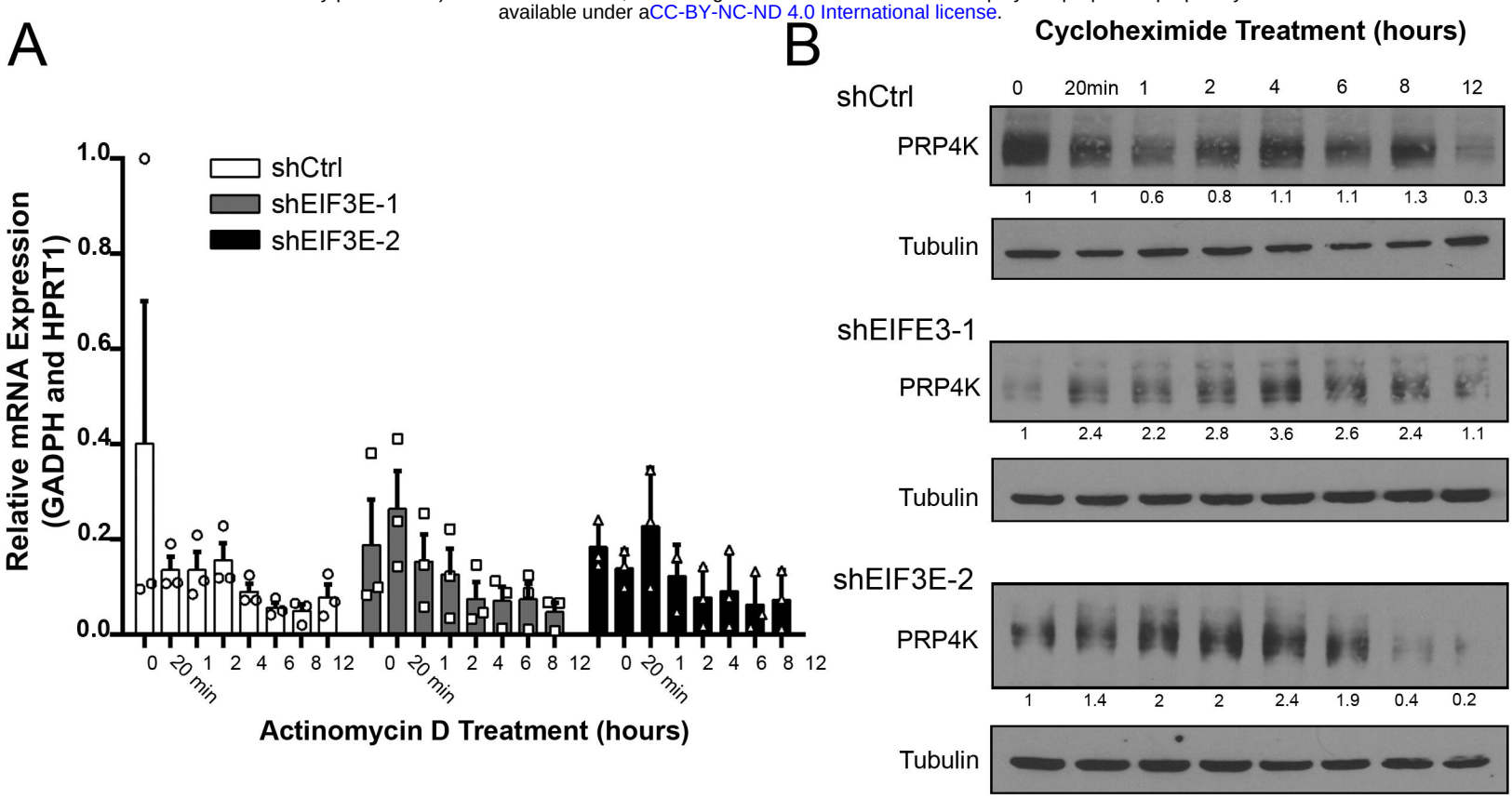

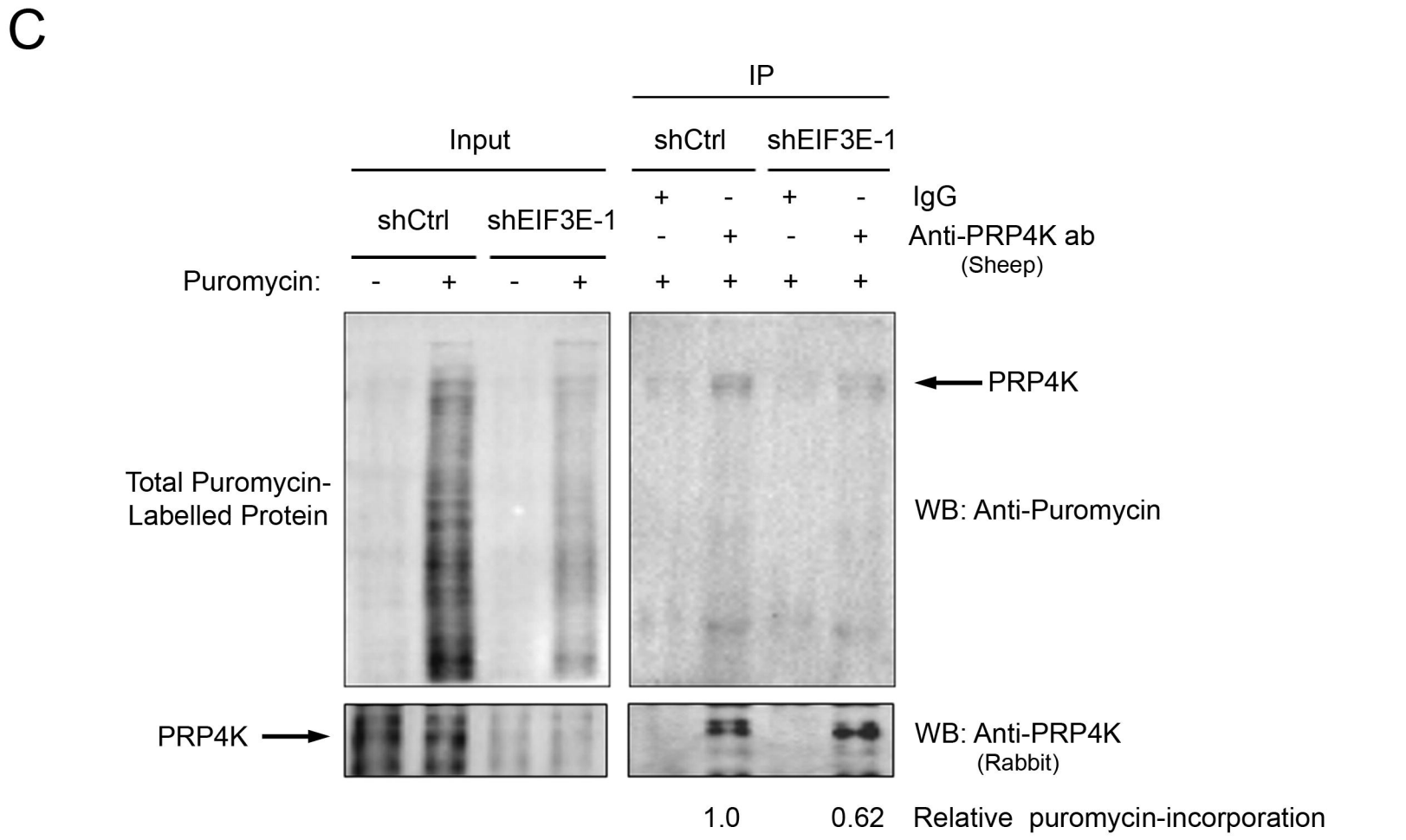

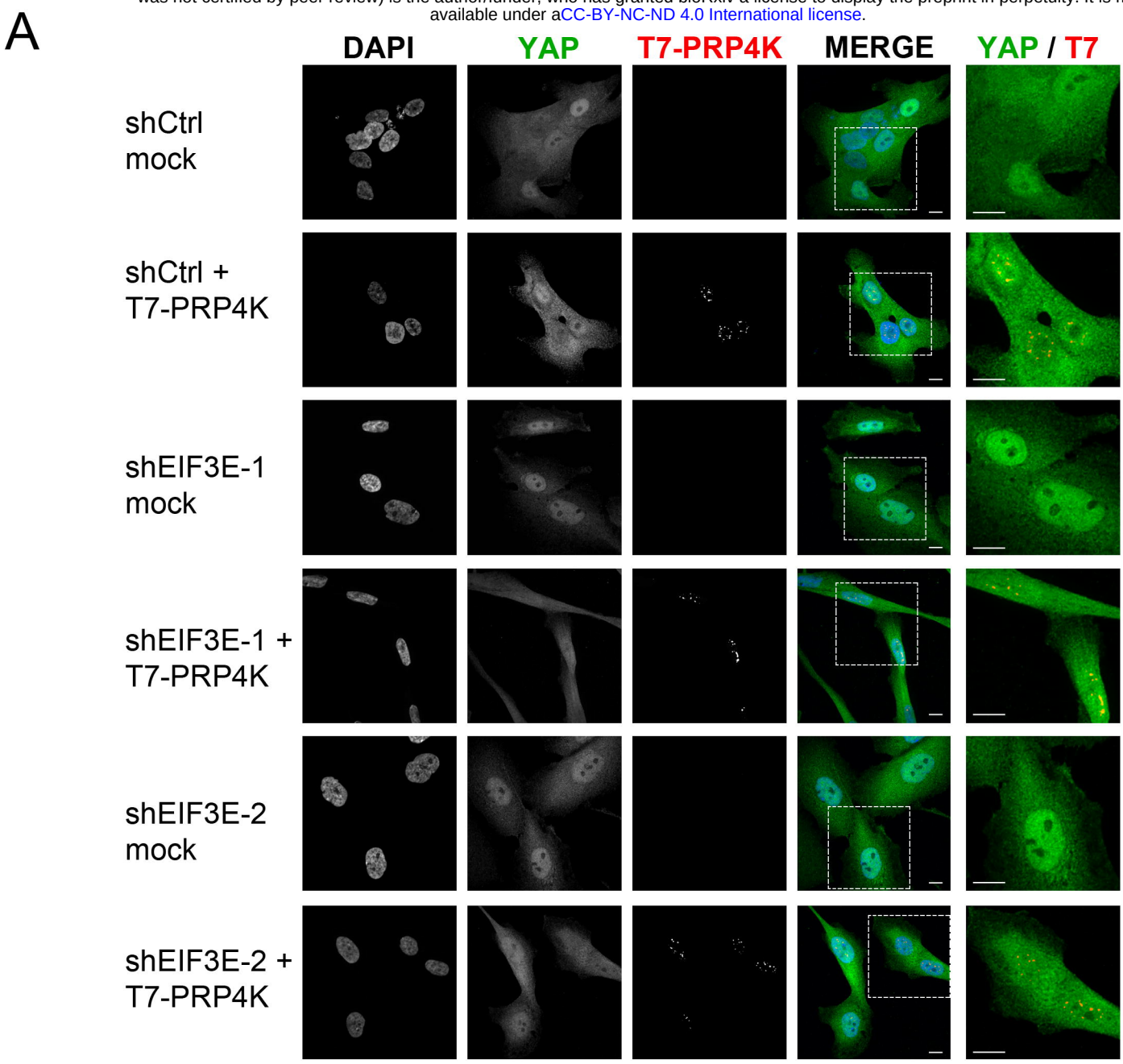

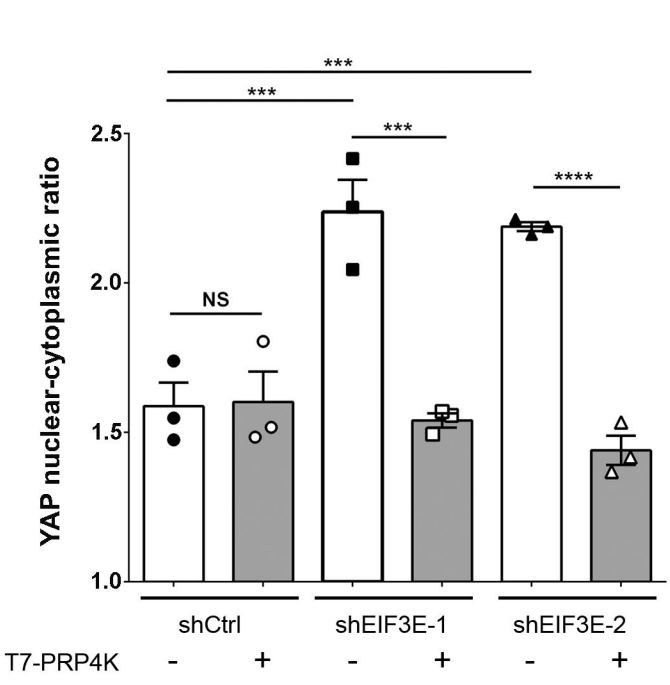

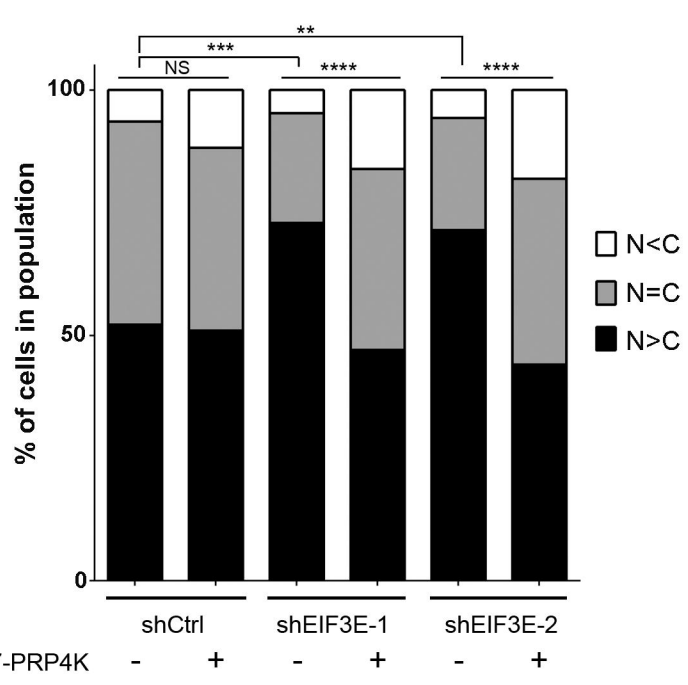

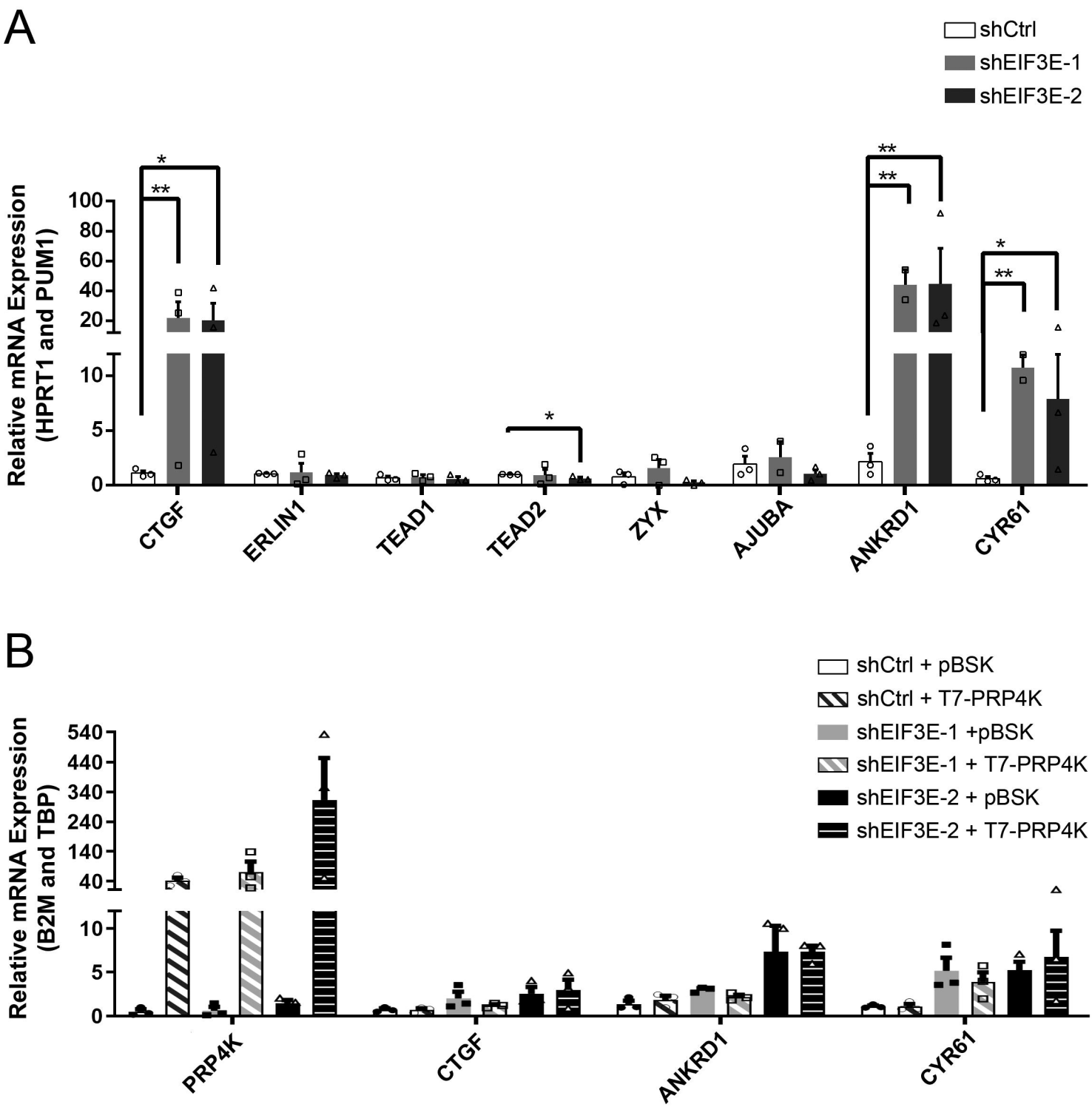

A

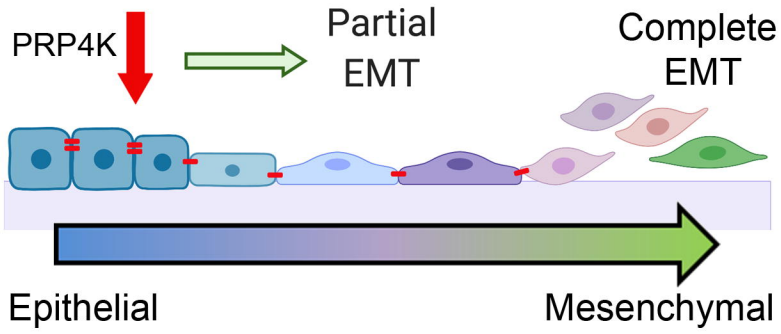

B